UNIVERSITY OF CALIFORNIA
Los Angeles

fMRI-iEEG Cross-Modality Supervised Learning for Epilepsy Presurgical Evaluation

A thesis submitted in partial satisfaction
of the requirements for the degree
Master of Science in Electrical and Computer Engineering

by

Trung Le

2020

© Copyright by
Trung Le
2020

ABSTRACT OF THE THESIS

fMRI-iEEG Cross-Modality Supervised Learning for Epilepsy Presurgical Evaluation

by

Trung Le
Master of Science in Electrical and Computer Engineering
University of California, Los Angeles, 2020
Professor Fabien Scalzo, Chair

Epilepsy - a neurological disorder characterized by recurring seizures - affects lives of more than 3.4 million Americans nationwide. Typical treatment procedure for patients resistant to anti-seizure medication involves invasive surgery to correctly characterize abnormalities in the epileptic network and localize epileptogenic zones by intracranial electrodes. Intracranial Electroencephalogram (iEEG) measured by this method provides a comprehensive way to monitor propagation of seizures and test hypotheses regarding the epileptogenic zones. However, the electrode implantation procedure poses unavoidable risks to the patients. Functional Magnetic Resonance Imaging (fMRI), on the other hand, is a non-invasive method providing another perspective on the epileptic network but does not have defining features for epilepsy analysis. It is of particular interest to find a link bridging the two modalities on the quest to have a comprehensive view of the network in epileptic brain. In this thesis we present a data-driven approach to find the mapping from fMRI-derived epileptic network to iEEG-derived epileptic network. We propose U-BrainNet, a deep learning model with special architectural considerations for cross-modality learning employing convolution operations specifically designed for connectomic data. We evaluate the model together with three other baselines on a population of 43 patients having intractable epilepsy, and provide insights into their performance as well as their feasibility to become clinically applicable with future modifications.

The thesis of Trung Le is approved.

Jonathan Chau-Yan Kao

Richard Joseph Staba

John M Stern

Fabien Scalzo, Committee Chair

University of California, Los Angeles

2020

To my beloved family,

who have always been by my side throughout this journey.

TABLE OF CONTENTS

LIST OF FIGURES

LIST OF TABLES

ACKNOWLEDGMENTS

I would like to express my deepest gratitude to my advisor, Professor Fabien Scalzo, for his valuable guidance and tireless support throughout the course of this thesis. His dedication and passion inspired me deeply, and his encouragement has been my great source of motivation during challenging times.

I also want to take this chance to especially thank Professor Richard Staba and Professor John Stern for providing helpful feedback and extending their expertise in epilepsy to shape the design of this study. I learned a lot from discussing with them, and I am forever thankful for that.

I would also like to thank Professor Jonathan Kao for agreeing to serve in my committee and offering his valuable comments. I am grateful for his class on Neural Networks and Deep Learning, which provided me the foundation to carry out this study.

My sincere appreciation also goes to Shawn Yeh and Mohamad Shamas for the insightful conversations and enjoyable brainstorming sessions. I am thankful for their work on data preprocessing, and for their help with the writing of section 3.2 in this thesis. I cherish every bit of our discussions trying to resolve issues along the course of this thesis.

Lastly, I would like to thank my dear family and friends. Without their love and constant support this thesis could never have been completed.

CHAPTER 1

Introduction

1.1 Overview and Motivation

Epilepsy is a neurological disorder characterized by recurring seizures causing abnormal sensations, uncontrollable motor behaviors, and loss of consciousness among many other symptoms. In 2015, it is estimated that 1.2% US population has active epilepsy [ZK17]. This means lives of 3.4 million adults and children are impacted by this disease nationwide [ZK17]. Due to the unpredictable nature of seizures, epilepsy significantly impairs the ability of affected patients to perform daily functions like driving and playing sports, and requires these patients to have frequent monitoring from caregivers. Seizures are abnormal electrical activities that originate from a local region of the brain and propagate throughout other parts of the brain network. The exact cause of epilepsy is largely unknown, and widely adopted treatments involve having the patient undergo resection of the epileptogenic zone after anti-seizure medications proved ineffective. Historically, epileptogenic zone is conceptually defined as "the area of cortex that is necessary and sufficient for initiating seizures and whose removal (or disconnection) is necessary for complete abolition of seizures" [LC01]. In order to locate epileptogenic zones, patients are first evaluated by a comprehensive set of non-invasive and invasive methods, including scalp Electroencephalogram (EEG), functional Magnetic Resonance Imaging (fMRI), Computed Tomography (CT), and intracranial EEG (iEEG) [DWK16]. From prevalent bio-markers and signatures these modalities show during both ictal phase (periods when seizures are occuring) and interictal phase (periods between seizures), neurosurgeons and epilepsy specialists decide the necessity of resection and determine the epileptogenic zones on which resection should be performed. The methods to

localize these epileptogenic zones are still an active field of research, and clinical success rate vary from cases to cases, depending on patient's conditions and complications [GE01] [DBP11]. Under this classical view of epilepsy, it is therefore crucial to have reliable methods for correctly localizing epileptogenic zones to assist presurgical diagnosis.

Contrary to this traditional belief of Luders et al. [LC01] where epileptogenic zone is thought to involve a focal source that acts as a "pacemaker" [WWH11], the view of epilepsy as a network disease has been increasingly adopted over recent years [BWE00] [ETS13] [WKC19] [Sta14]. This view suggests that epilepsy is characterized by aberrant functional connectivities between brain regions and that this abnormal network once modulated or inhibited could theoretically suppress epileptic activities [WWH11]. These abnormalities can be captured under various modalities, both invasive and non-invasive, although their integrity and resolution are subject to the nature of the recording method. Some prior works using fMRI have found increase or decrease in network synchrony as measured by graph theory based network parameters in different parts of the epileptic brains compared to healthy controls [HCY15] [HLY14]. Others have found relationship between postoperative outcomes and gamma coupling events as measured by iEEG in areas ipsilateral to the onset zone [AAW15]. These findings suggest that functional brain networks could hold valuable features predictive of the initiation and propagation of epilepsy seizures [SDK17].

Since the 1960s, intracranial electroencephalogram (iEEG), known as stereotactic electroencephalogram (sEEG) if using depth electrodes or electrocorticogram (ECoG) if using subdural grid electrode, has been the gold standard in epilepsy diagnosis [PK18] [BLW17]. sEEG method, as used in this thesis, consists of multiple intracerebral electrodes covering interested brain areas and allows for a continuous electrophysiological monitoring of the onset and propagation of seizures [BLW17]. Epilepsy specialists could test their hypotheses by sampling (implanting) depth electrodes at suspected regions backed by data collected by non-invasive methods and observe electrical activities at each implanted area and the network organization among them. Thanks to its high temporal resolution (up to 500Hz) [UCD07], sEEG is favorable for real time investigation and analyses at a fine time scale. However, their sampling coverage is limited, while their invasive implantation requires close

monitoring and hinders applicability in patients with risks of complications. fMRI, on the other hand, measures hemodynamic response via Blood Oxygen Level Dependent (BOLD) signal and provides whole brain spatial resolution in exchange for lower temporal resolution (on the scale of seconds) [Glo11]. Each modality offers a unique perspective on the brain dynamics and network structure, and both have proven benefits for epilepsy diagnosis [SZY20] [NSN18].

It is therefore of particular interest to find a link bridging the two modalities on the quest to have a comprehensive view of network in epileptic brain. We would like to have the perk of whole brain coverage and non-invasiveness brought about by fMRI while also enjoying the unparalleled high integrity measurements of iEEG. A predictive model capable of picking up abnormalities in network functional connectivities captured by fMRI and translating them to iEEG features, if exists, would be of great value for the presurgical evaluations of epilepsy as it will garner the strengths of both modalities without the need of invasive implantation. In this thesis, we will tackle this challenge from a data-driven approach. We propose to use state-of-the-art machine learning architectures to investigate the existence of this fMRI-iEEG cross-modality relationship under the definition of epilepsy as a network disease. Concretely, we attempt to learn a common cross-modality representations interrelating fMRI and iEEG networks that can be used to predict iEEG network connectivity measures from fMRI counterparts, using data collected from 43 patients with intractable temporal lobe epilepsy. The reconstructed iEEG network features will serve as a reference point for neurosurgeons and specialists to conduct further analyses and identify abnormalities in epileptic network whose suppression by surgery could help abolish seizures.

1.2 Contributions

The main contributions of this thesis are the following:

- A deep learning model, U-BrainNet, leveraging special architectural design suited for cross-modality learning, as well as convolution operations specifically designed for connectomic data to effectively extract graph features. Three other baseline models were

also proposed to compare performance of U-BrainNet.

- An extensive evaluation on fMRI and iEEG connectomic data to search for a mapping between fMRI-derived epileptic network and iEEG-derived epileptic network. This study, to the best of our knowledge, is the first ever attempt to bridge the gap between these two modalities and to encourage a non-invasive method for epilepsy network analysis.

1.3 Thesis Organization

The organization of this thesis is as follows. First in chapter 2 we introduce traditional methods used by the research community to localize epileptogenic zone and recent approaches to identify abnormalities in epileptic networks. We will also discuss nascent efforts of applying deep learning model on graph based data applicable to brain connectome. In chapter 3 we will present the detailed description of our proposed deep learning architectures, the reasoning behind our design selection and the experiments conducted to demonstrate its applicability. In chapter 4 we will present evaluation results of our method and comparison of different models. We will take a deeper look into the results, offering our speculations and discussions on the current and future work in chapter 5, and provide conclusions in chapter 6.

CHAPTER 2

Background and Related Work

2.1 Functional Magnetic Resonance Imaging

Functional Magnetic Resonance Imaging (fMRI) is a non-invasive method to measure neural activity indirectly via the change in blood flow. Since its inception in the 1990s, fMRI has been widely adopted to study neurological disorders and assist in clinical advancement of care [Glo11]. fMRI measures the Blood Oxygen Level Dependent (BOLD) contrast resulted from the change in magnetic property of hemoglobin when oxygenated and deoxygenated [Glo11]. Oxygenated hemoglobin is diamagnetic while deoxygenated hemoglobin is paramagnetic [Glo11]. Following a neural activation, oxygen-rich blood (oxygenated hemoglobin) rushes to the activated area, altering the magnetic field which is in turn picked up by fMRI scanner [Glo11]. Since there is a couple of seconds delay between stimulus and blood flow response, activities captured by fMRI only partially reflect neural activations at the high level [Glo11]. In fact, fmRI is limited in temporal resolution and has low signal-to-noise ratio, lending back to the longer scan duration as a trade-off for smaller voxels (higher spatial resolution) [MBB07]. On the other hand, fMRI is non-invasive, radiation-free, offers a view of the whole brain and enjoys high spatial resolution down to 3 mm [YTG04]. Overall, despite its shortcomings, fMRI is still capable of capturing signatures within the brain network and is widely used to assess abnormalities in the epileptic brain [SLS11].

2.2 Intracranial Electroencephalogram

Intracranial Electroencephalogram (iEEG) is an umbrella term for stereotactic electroencephalogram (sEEG - as used in this thesis) and electrocorticogram (ECoG) [PK18]. The difference between sEEG and ECoG is the use of depth electrodes in the former and subdural grid electrodes in the latter. Earliest use of sEEG dated back in the 1960s with the work of Tailarach and Bancaud [BTB65]. sEEG since has increasingly been adopted by the epilepsy community and has become a gold standard to test hypotheses on potential epileptogenic zones [BLW17]. It is worth noting that sEEG is only used after non-invasive recording methods fail to localize apparent lesions and the implantation locations of electrodes follows biomarkers as seen from non-invasive data [BLW17]. The electrodes are typically implanted at 8-15 locations depending on the need of each study, with multiple contacts 2 mm long and 1.5 mm apart along a 0.8 mm diameter electrode [BLW17]. This configuration of sEEG allows for multiple-site simultaneous recording of electrophysiological activities, which proves valuable for epilepsy presurgical planning. The prevalent employment of sEEG in various epilepsy studies also supports the notion of epilepsy as a network disease, since although in some cases seizures have been observed to be confined to a restricted area (conforming with classical view of epilepsy by Luders et al [LC01]), most of the cases we see discharges erupt simultaneously at multiple regions or very rapidly involving several distributed regions, hinting that a network model might be a more accurate description for the disease. [BLW17]. As mentioned before, sEEG reflects closely the neural activities but has poor spatial sampling. Practical value of sEEG data depends heavily on whether the electrodes are implanted at the locations optimal for analysis [BLW17].

2.3 Machine Learning Approaches in Epilepsy Diagnosis and Presurgical Planning

Machine learning, a subfield of artificial intelligence, has been widely adopted in biomedical studies for tasks where there exists a need for statistical modeling and extracting non-trivial

features from data. Taking advantage of an increasingly abundant labeled medical data, supervised learning has thrived as an effective tool to learn data representations based upon which predictive decisions could be made. With regards to epilepsy, supervised learning has been used to predict epileptic seizures [KH20] [FHH16], surgical outcomes [AMS14], [MKD15], [SDK17], onset zones [HAZ18] and epileptogenic zones [NSS18] [EYM17]. The algorithms can be applied on time-series data, frequency-based or graph-based features using any electrophysiological or imaging modality pertaining to the nature of the study. A wide variety of machine learning techniques have been employed, most of which are classifiers, ranging from Support Vector Machine (SVM) [ZP14] [AMS14] [NSS18] [MKD15] [TMP17], k-nearest neighbor [FHH16], random forest [MZC17], and deep neural network [GMB18] [HAZ18] [HTP17]. The procedure typically involves a preprocessing step where electrical and imaging data are filtered for remove undesirable noise and artifacts such as electric line interference and head motion during scanning. Usually some forms of data augmentation is also performed for studies with limited labeled data. Corresponding algorithm is then employed to train the model and the performance is evaluated using cross-validation.

Machine learning methods are preferable in cases where there is a non-trivial relationship between underlying data and prediction target that goes beyond human reasoning (discovering sophisticated features) or would require extensive expert investigation (where automation is preferred, as in the case of automatic seizure detection). Despite promising results as reported by high classification accuracy and area under curve (AUC) in some studies, challenges still remain. One of the most prominent problems is the limited access to medical data, which cripples the predictive ability of the machine learning model and makes the model susceptible to overfitting. Following the exemplars of large publicly available datasets such as ImageNet [DDS09] that have revolutionized the field of deep learning for object recognition, large databases are being established for epilepsy research, for which the European Epilepsy Database is an example [IFT12]. However, most of the current epilepsy studies are still limited by the small sample size, typically a couple dozens, hence raise many questions on their statistical significance and reproducibility on a larger population.

2.4 Supervised Cross-Modality Learning

2.4.1 Assumed Correlation Between Resting State fMRI and Interictal iEEG

As stated in the introduction, this thesis focuses on finding the correlation between fMRI and iEEG within the scope of epilepsy diagnosis. We adopt the notion of epilepsy as a network disease, where abnormal functional connectivities within different brain regions in the network, rather than a single epileptogenic region, give rise to the initiation and propagation of seizure [PMS14]. The link if established would map the fMRI connectivity features to iEEG counterparts and lends itself on the assumption that such a link exists. We know, however, that the electrophysiological signal of iEEG and BOLD signal of fMRI both reflect the underlying activities at the neuronal level, thus their measured functional connectivity would potentially relate to each other. This theory is supported by a study conducted by Stufflebeam et al [SLS11], where they found the foci identified by fMRI overlapped with the epileptogenic region identified by iEEG. For fMRI, the foci was determined as areas having above-threshold average Pearson correlation with the rest of the brain. For iEEG, epileptogenic zones are identified as regions where seizure onset happens and regions with high interictal acitivities. Zhao et al [ZWW19], on the other hand, calculated Epileptic Index (EI) from iEEG gamma band and set regions with high EI as seeds where fMRI correlations of seed regions with other regions were obtained. They found that the network of regions having high EI overlapped with the fMRI network highly correlated with the seed region. Vulliemoz et al [VCR11], Khoo et al [KHE17] also confirmed the concordance between interictal epileptiform discharge (IED)-related BOLD response with the foci localized by iEEG. These findings, although differ by analysis methodology and analysis procedure, suggest that fMRI BOLD signal and iEEG electrical signal are correlated on different levels with respect to the epileptogenic zone. These studies requires plenty hand-crafted features and are already biased towards current knowledge about epilepsy - which might or might not be correct. There could be more abnormalities in the network that might contain valuable information for epilepsy diagnosis but went overlooked or omitted. This thesis attempts to predict full iEEG epileptic network from corresponding fMRI functional network, preserving abnormal-

ities within it that experts could refer to without the need of invasive surgeries to implant iEEG electrodes. The proposed machine learning model could be trained to reconstruct network as defined at different frequency bands as per the need of human investigators.

2.4.2 State-of-the-Art Cross-Modality Supervised Learning Methods

Cross-modal learning has gotten special attention in the last decade thanks to the wide range of potential applications and recent advances in deep neural networks. It allows retrieval of one modality given a query of another modality. The underlying basis for the feasibility of this retrieval is that the modalities despite being different by its own nature all share a same semantics. For example, an image of a cat, a video showing the cat playing with a ball, and an English sentence describing the scene are different ways of depicting the same subject which is the cat. The goal of cross-modal retrieval is to allow users to submit an instance of one modality, e.g. an image, and obtain corresponding relevant results in other modalities, e.g. audio, video, text description, 3D models, etc. Cross-modality retrieval has been an active field of research for the last several decades, and multiple techniques have been proposed to address the problem, ranging from linear methods to deep learning based varieties. For a comprehensive review, see [PHZ17].

One key challenge in cross-modality learning is the so-called "heterogeneity gap" which means the representation and data distribution of each modality lie in distinct feature spaces thus make it difficult to measure the similarity between samples of different modalities [PHZ17] [HZP19]. To tackle this challenge, multiple methods have been proposed over the years, which can be classified into to two large categories: traditional statistical methods and deep learning methods [HZP19]. Traditional methods are largely based on Canonical Correlation Analysis (CCA). Given two random variables, CCA finds linear combinations of the random variables such that these combinations have maximum correlation. Thanks to this power, CCA is well suited for cross-modal retrieval task since it projects data of different modalities to a common subspace that maximizes the correlation between the original two heterogeneous datasets [HSS04]. As CCA is inherently a linear method, it cannot model well

complex correlations with high nonlinearity [HZP19]. Some works have extended CCA with kernel trick to overcome this limitation [Aka06]. The second category of cross-modal learning methods utilizes recent advances in deep neural network to learn complex mapping projecting one modality to the others. Convolutional Neural Networks (CNN), Recurrent Neural Networks (RNN) - especially Long-Short Term Memory (LSTM), Variational Autoencoder (VAE) and Generative Adversarial Networks (GAN) have been used in tasks such as 2D-3D modeling [SSP18], video/image captioning [RAY16] [CAV16], and image style transfer [IZZ17] [SZC20] [ZPI17].

Our problem of inferring iEEG-derived network from fMRI-derived network in epileptic brain can be formulated as a cross-modal learning task. Deep neural networks based cross-modal learning is increasingly adopted for biomedical applications. Encoder-decoder framework is sometimes employed in these works. This framework attempts to find a common feature space encoded by the encoder which can subsequently be mapped back into the modality of interest by the decoder [JLC19] [KKS17]. Among the most notable encoder-decoder architecture successfully applied to biomedical data is U-Net [RFB15], which is originally developed to tackle segmentation of neuronal structures. Other cross-modality prominent works include [Han17] [GWX19] [JHT19]. The name lends itself to the U-shaped architecture, which involves multiple layers of convolution and transposed convolution operations. The middle of the architecture (the so-called bottleneck) can be seen as the compressed representation of the input data. Copies of feature spaces in the encoder stages are copied to respective layers in the decoder stages. The intuition is that features learned by encoder will assist the reconstruction in the corresponding stages of the decoder. In this thesis, we take inspiration from the design of U-Net to develop one of our custom models.

2.5 Deep Learning on Connectomic Data

Our work closely relates to computational methods done on connectomic data, since we are trying to find the correlation between fMRI-derived network and iEEG-derived network. A connectome is defined as the map of connection between brain regions. Mathematically, a

connectome is a NxN matrix of N brain regions, where each cell A_{ij} expresses the strength of connectivity between region i and region j. Connectivity are mostly computed using Pearson correlation. Connectomic data has some special properties that make it unique from other types of data and pose challenges for deep neural network compatibility. Firstly, the connectome is essentially a graph whereby nodes are brain regions and edges represent connectivity strength. Since a graph is isomorphic, i.e. nodes and edges can be moved around within the topology of the network without changing the properties of the network itself, order of rows and columns in the connectivity matrix should not factor in during the learning. However, deep neural network treats the connectivity matrix as an ordered structure where spatial information of the cells matters. Thus, successful traditional convolution operation in CNN, which is done on a crop of the matrix and was meant to extract local spatial information of the image matrix, does not provide meaningful interpretation anymore. Secondly, the connectome is usually a huge network containing thousands of nodes, while unlike image processing where images are abundant and somewhat easy to obtain, medical data is very limited, often on the order of dozens samples per study. Training on connectomic data is proned to overfitting, thus requires architectures to be simple and to employ of some regularization methods.

Research on deep learning based methods applicable to connectomic data is still at an early stage. Ju et al [JHL17] uses a stacked autoencoder to learn discriminative features from resting-state fMRI connectome that can separate Alzhelmer's brains from normal aging ones. They also found that the brain connectome contains information more discriminative than the time-series data. Kim et al [KCS16] proposed an autoencoder architecture with L1-norm regularization and found that sparsity constraints imposed by the regularization improved the performance on schizophrenia classification. These works vectorized the NxN square connectivity matrix into an Nx1 vector and treated it as the input to the deep neural network. This method of input transformation discarded the topology of the brain network and impose unnecessary and wrongful assumption on the order of nodes in the input vector. In the domain of computer vision, CNN [LBH15] has been proposed that efficiently learns the spatial local information in grid-like data like images. Taking inspiration from this,

Kawahara et al [KBM17] proposed BrainNetCNN which includes a connectome-compatible convolution operation that learns the edge-to-edge and edge-to-node relationships. Meszlenyi et al [MBV17] further improved this convolution mechanism by exploiting the multi-channel convolution technique [XJY18]. Xing et al [XJY18] made another modification to the convolution operation by Kawahara et al to allow each edge to have different weights rather than sharing weights in the original technique. There has not been many works tackling the problem of reconstructing a connectome from a connectome of another modality. We note, however, a work by Bessadok et al [BMR19] which proposed a GAN architecture to predict a target brain graph from a source graph, is an early attempt to tackle the similar problem we are tackling in this thesis.

CHAPTER 3

fMRI-iEEG Cross-Modality Learning

3.1 Problem Formulation

In this section we are going to lay out some prerequisite definitions and fundamental concepts that would provide some background and help us formulate the problem formally.

Definition 3.1. (Functional Connectivity) Functional connectivity is the temporal dependency of neuronal activation patterns of anatomically separated brain regions. [VP10]

Remark 3.1. *Functional connectivity is measured by statistical methods employed on time-series data. This term is to be distinguished from a closely related term of "structural connectivity", which is defined as the existence of white matter tracts physically interconnecting brain regions [Udd13]. Two brain regions showing functional connectivity do not necessarily have structural connectivity and vice versa.*

Functional connectivity is most commonly measured by Pearson's correlation coefficient, which is mathematically defined below:

Definition 3.2. (Pearson's correlation coefficient)

$$\rho_{XY} = \frac{Cov(X,Y)}{\sigma_X \sigma_Y} = \frac{E[(X-\mu_X)(Y-\mu_Y)}{\sigma_X \sigma_Y} \tag{3.1}$$

where

- X, Y are two random variable
- ρ_{XY} is the Pearson's correlation coefficient of X and Y
- $Cov(X,Y)$ is the covariance of X and Y

- E is the expectation
- σ_X, σ_Y are standard deviations of X and Y, respectively
- μ_X, μ_Y are mean of X and Y, respectively

When working with connectomic data, some basic definitions from graph theory are helpful:

Definition 3.3. (Graph) A graph is a pair of sets (V, E), where V is the set of vertices and E is the set of edges, formed by pairs of vertices. [Ruo13]

Definition 3.4. (Undirected graph) A graph is an undirected graph if its edges are an unordered set of two vertices.

Definition 3.5. (Graph isomorphism) Two graphs G_1 and G_2 are isomorphic if there exists a matching between their vertices so that two vertices are connected by an edge in G_1 if and only if corresponding vertices are connected by an edge in G_2. [Laz]

Remark 3.2. *The brain network can be treated as a graph where vertices are brain regions and edges are functional connections between two regions. Since we are using Pearson's correlation to represent the strength of edges, the graph is undirected, i.e. there is no notion of causal effect of one region on another. Since all isomorphic brain networks essentially represent the same network, the cross-modality algorithm should take this fact into account to facilitate effective learning. Later on in this chapter we will present how we encouraged learning of isomorphic graphs by augmenting the data with permuted versions of itself.*

Problem formulation: For our deep learning approaches, we formulate the fMRI-iEEG cross-modality problem as predicting the connectivity map of iEEG $Y^{N\text{x}N}$ given a connectivity map of fMRI $X^{N\text{x}N}$. Concretely, the input to the model is the connectivity matrix computed by Pearson's correlation of fMRI time-series data in the frequency band of interest:

$$X = \{\{X_{ij}\}|A_1, A_2, ..., A_\tau\}, \qquad i, j \in \{1, 2, ..., N\}$$

where A_t is BOLD activation map of fMRI at time t, N is number of considered regions where we have iEEG electrode implanted.

The respective ground truth target is the connectiviy matrix computed by Pearson's correlation of iEEG time-series data in the frequency band of interest:

$$Y = \{\{Y_{ij}\}|B_1, B_2, ..., B_{\tau'}\}, \qquad i, j \in \{1, 2, ..., N\}$$

where B_t is all-channel eletrophysiological iEEG signal at time t.

We attempt to predict a connectivity matrix $\hat{Y}$ resembling the ground truth by the deep neural network:

$$\hat{Y} = f(X; W)$$

where W is the set of weights in the deep neural network.

3.2 Subjects and Data Preprocessing

3.2.1 Subjects

Medical data of 43 patients used in this thesis was obtained in the framework of UCLA Adult Epilepsy Surgery Program. The clinical data used for analysis was anonymized, removing identifiable personal information. Patients admitted through the program had chronic limbic seizures that were resistant to anti-seizure drugs. The patients underwent non-invasive tests including brain imaging (fMRI and PET), interictal and ictal scalp EEG, neurocognitive tests, and source localization to localize epileptogenic network (EN). During fMRI scanning sessions, subjects are instructed to relax and lie still eyes open. If the EN localization results from these tests are unequivocal, subjects would go for resective surgery directly. However, if the EN could not be localized to a restricted region of mesial temporal structures on one side, invasive tests were recommended. Depth electrodes were then implanted at all of the suspected regions of EN. Electrodes are always implanted bilaterally to monitor propagation pattern of seizure and distinguish mesial from neocortical seizure onsets, even when EN was lateralized by non-ivasive methods. iEEG signals were recorded over a period of 10-14 days to adequately capture habitual onsets, with typically 200Hz sampling rate. Lastly, the subjects would undergo resective surgery and follow-ups to determine post-surgery outcome.

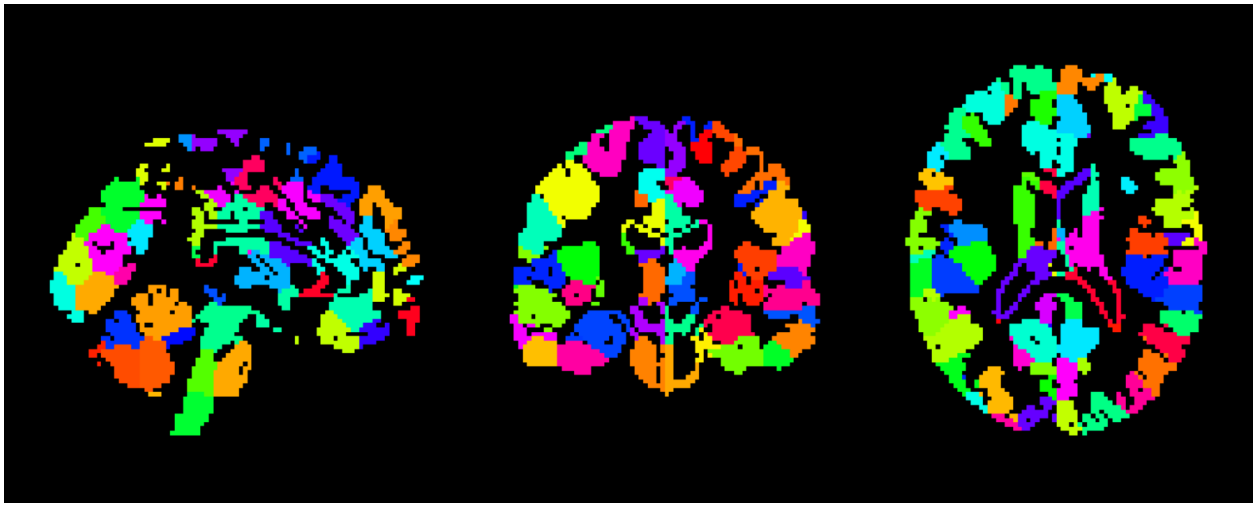

Figure 3.1: Shen atlas dividing the brain into 278 ROIs [STP13].

3.2.2 fMRI preprocessing

We follow the same data acquisition and preprocessing procedure in [CCG16] for fMRI time series data. Resting-state fMRI imaging was done using 3T MRI scanner. Each scan lasted for 4 to 8 minutes. DICOM images containing CT, structural and BOLD scans were converted to Nifti format and processed using fMRIB Software Library (FSL) [JBB12]. Head movement artifact correction was performed using FSL motion outliers tool. Additional processing include high pass filtering, spatial smoothing, non-brain tissue elimination [Smi02] [CCG16]. The resulting time series were then band-pass filtered at 0.01Hz-0.2Hz. We used a 278-region Shen atlas [STP13] (Figure 3.1) to co-register the de-meaned time series in MNI 2mm space. Each region of interest (ROI) in the resulted atlas consists of many voxels, thus we took the average of all voxels falling within the ROI boundary to represent that ROI. We then obtained connectivity matrices by computing Pearson's correlation of each ROI time series to all other ROI time series using a sliding 88-second-window with a 50% overlap. Therefore we obtained multiple connectivity matrices for the same patients, each connectivity matrix is correlation of time series during corresponding 88s window. In another separate thread, we co-registered CT and structural scans, then highlighted electrode contact locations on the structural scan using a combination of thresholding and Gaussian kernel filters (Figure 3.2). The resulting image with electrodes highlighted was loaded into

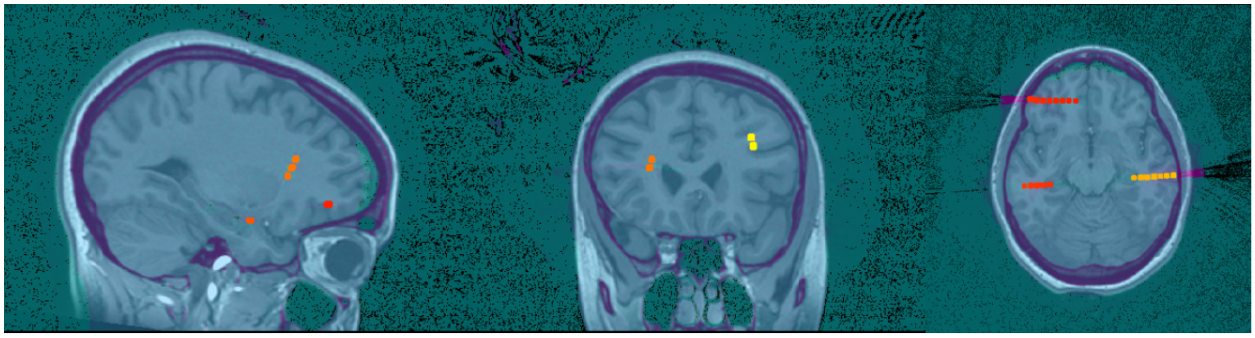

Figure 3.2: Electrodes overlaying on structural scan.

iElectrodes [BPP17] for labeling and indexing. For later analysis of cross-modality learning models, we extract only ROIs where at least one electrode is implanted rather than using the whole brain map.

3.2.3 iEEG preprocessing

iEEG signals from electrode contacts are often contaminated with noise. Noise can come from a variety of sources, including powerline interference and equipment systematic noise. Uncontrollable movements of patients during seizures might also loosen the contacts and contribute to the loss of channels during the recording process. We visually inspected and manually selected iEEG channels to ensure its high signal integrity. Heavily noise-contaminated channels were excluded from analysis. We applied a 60 Hz notch filter to attenuate strong powerline interference. Several electrode contacts may fall into one ROI, thus we took the average of time series of those contacts to be the representative time series for that ROI. For each patient, we computed connectivity measures using 10-minute windows. Similar to fMRI, the connectivity measure we used was Pearson's correlation for filtered signal at the low gamma band (30-60 Hz), i.e. we band-pass filtered all time series at low gamma band and computed Pearson's correlation of the time series of all ROIs, although it might as well be any other measures such as gamma coupling event [AAW15], graph measures like edge betweenness centrality, or Pearson's correlation in other frequency bands. This connectivity measure extraction process resulted in multiple connectivity matrices. Since recording time for each patient varied, the number of possible 10-minute windows also varied. We chose

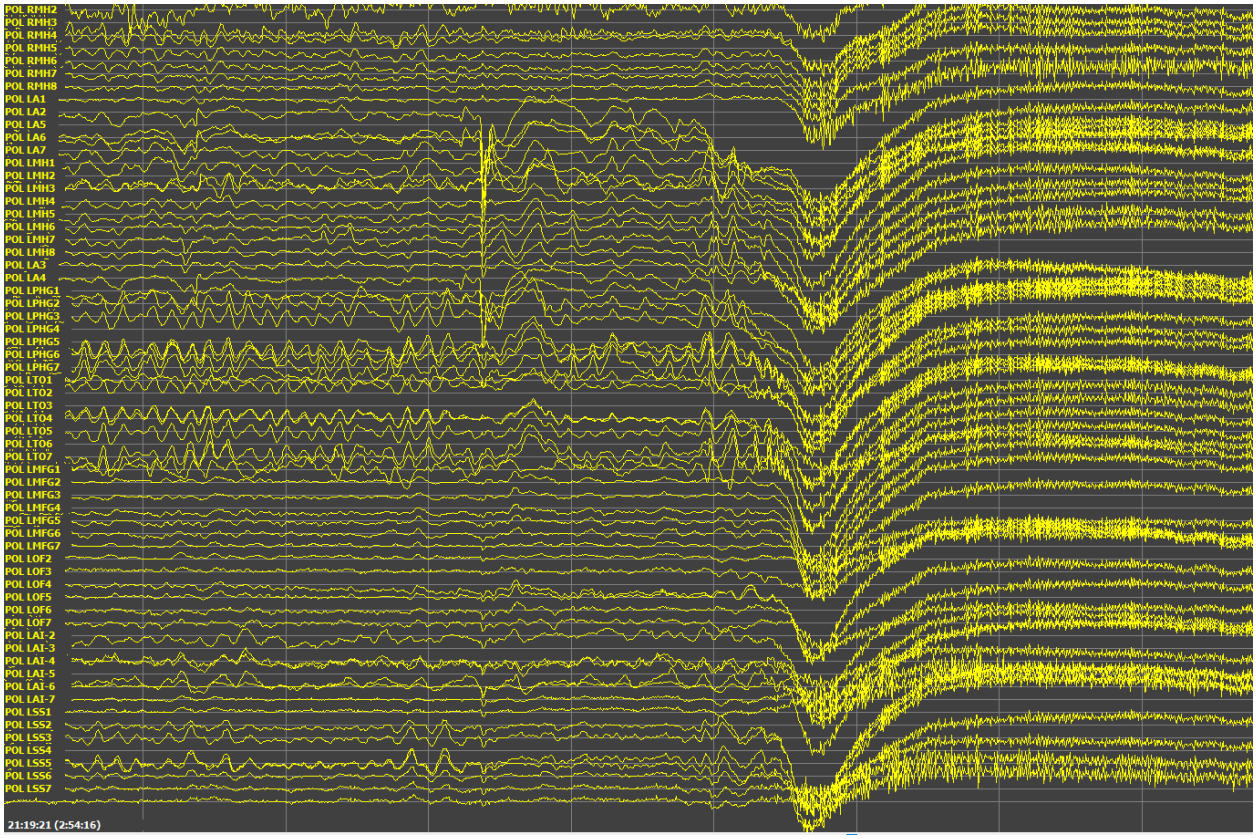

Figure 3.3: Time series of iEEG signal showing abberant activities right before seizure. It can be seen that the seizure starts from electrodes on the left hemisphere (LA1-4, LMH5-7) then spreads all over the brain network.

the number of iEEG connectivity matrices to be the same as that of fMRI, and the same as the minimum available matrices for the patient with the shortest fMRI recording time. This is to ensure data balance, i.e. each patient epileptic network contributes the same amount of data to the training and validation set. Note that by using the sliding window approach to create multiple fMRI and iEEG connectivity matrices for the same subject, we also essentially increased the size of our data, which would help the training of the deep neural network model.

3.3 Pairwise Connectivity Level Prediction

First we would like to test the hypothesis of whether there exists a mapping on the pairwise connectivity level, in other words, if an individual strength of an edge in fMRI network can directly predict the strength of that edge in the iEEG network. Essentially we want to find a mapping

$$\mathcal{M} : \mathbb{R} \mapsto \mathbb{R} : \mathcal{E}_{ij}^{fMRI} \mapsto \mathcal{E}_{ij}^{iEEG}, \forall i, j \in \mathcal{V}$$

where $\mathcal{E}_{ij}$ is the strength of the edge between vertex i and vertex j as measured by Pearson's correlation, and $\mathcal{V}$ is set of vertices of the considered network.

Since the connectivity matrix is symmetric, we took only the upper triangle of the matrices to be our inputs and targets. The minimum number of ROIs having implanted electrodes is 16. Some subjects have electrodes in more than 16 ROIs, but in order to have a consistent input size for all subjects, we chose 16x16 as the dimension of the connectivity matrix. In subjects having more than 16 ROIs, we randomly chose 16 ROIs among them and treat as if the rest were never implanted. Although we are discarding some available data this way, it is also important to note that even if do include them all, there is still a risk of not having the "important"/"significant" ROIs that truly hold the abnormality in the brain network. This is a limitation of iEEG that we have to live with. iEEG can never have a whole brain coverage as fMRI. We also note however, to mitigate the amount of data discarded, we could have considered all combinations of 16 ROIs among N available ROIs, so that we will end up having $\binom{N}{16}$ connectivity matrix rather than just one. However, this will result in subjects having large number of available ROIs dominating the dataset, creating data imbalance. We therefore only selected a random combination of 16 ROIs among N ROIs to ensure all subjects are equally represented in the training set. Thus after extracting the upper triangle of the 16x16 connectivity matrix and vectorize it, we have a vector of $\binom{16}{2} = 120$ elements. As mentioned before, we used a sliding window approach to extract multiple connectivity matrices from the time series of fMRI and iEEG. Since fMRI sampling rate is low (2s per scan), we used a 88-second-window with 50% overlapping to ensure the window length covers enough samples and remains relatively stable across windows. We could apply minimum of 3

windows on the patient with shortest fMRI scan. Some patients with longer scans can have more windows, and thus connectivity matrices, extracted. However, similar to how we chose the number of ROIs for the connectivity matrix, we selected 3 windows for each patient to ensure data balance. Overall, each patient has 3 16x16 connectivity matrix, and we have totally 43 patients, resulting in 3*120*43 = 15480 data points for each modality.

Since our data is a 1-D vector, the problem of finding the edge-to-edge pairwise mapping from fMRI to iEEG can be tackled by any regression method. We initially chose Ridge Regression as our method. Ridge regression is a linear regression method with an L2 norm regularization term to minimize the magnitude of the coefficients, which will stabilize the model and reduce the model variance. Given a target vector $y \in \mathbb{R}^n$ and predictor matrix $X \in \mathbb{R}^{nxp}$, Ridge regression coefficient is defined as:

$$\hat{\beta} = \underset{\beta \in \mathbb{R}^p}{\operatorname{argmin}}(||y - X\beta||_2^2 + \lambda||\beta||_2^2)$$

where λ is a hyperparameter setting the regularization strength [Tib]. $\lambda = 0$ means

In our problem, $y \in \mathbb{R}^{15480}$ and $X \in \mathbb{R}^{15480\text{x}1}$. We standardized X and y before fitting the regressor. We did not find a good fitting on this pairwise connection prediction. We will provide details about the results and a visualization giving insights into the data distribution that may explain the poor fit in chapter 4.

3.4 Connectome Level Prediction

In contrast to the pairwise edge-to-edge connectivity prediction as presented above, we also attempted to find the correlation of fMRI-iEEG network on the connectome level. Essentially, we now assume the strength of an edge in iEEG connectivity matrix not only depends on the strength of the corresponding edge in the fMRI connectivity matrix, but depends instead on the collective activities of all edges in the fMRI network. The problem now comes down to learning the abstract inter-relationship between edges in the fMRI network that would affect each edge in the iEEG network. Deep neural networks are well-suited for this type of prediction as it has great ability in learning complex mapping functions. In the following

sections we will present four neural network models built to solve this problem. We will describe their architecture in this chapter and provide comparison on their performance in chapter 4.

Encouraging learning of isomorphic graphs: As mentioned earlier in this chapter, all isomorphic graphs (connectivity matrices) represent the same brain network. The order of columns and rows in the connectivity matrix should not matter when it comes to learning abstract features characterizing abnormalities in the epileptic network. However, neural networks take ordering of cells in the input matrix into account when learning. Therefore if we only teach our deep neural network models one instance of these graphs, the models may miss out on other isomorphic graphs and becomes heavily biased on the configuration it was taught. We encouraged the learning of isomorphic graphs by generating multiple isomorphic graphs. This is done by permutating of the order of columns and rows in the connectivity matrices. For a 16x16 matrix, there is 16! = 2e13 ways of arranging columns and rows, thus it is computationally impossible to learn from all these configurations. We thus selected 100 permutations from this 16! set. Aside from making the neural network aware of isomorphic graphs, this method also allow us to obtain more training data, effectively increasing the training size 100-fold.

3.4.1 Shallow Fully Connected Network

As a baseline for other models presented later in this chapter, we built a shallow fully connected neural network consisting of three layers. The input to the network is the vectorized upper triangle of the fMRI connectivity matrix, and the output of the network is the vectorized upper triangle of the corresponding iEEG connectivity matrix. Hence, the input and output layers of the fully connected network is set to 120 neurons. We also set the size of hidden layer to be 120. A visualization of the shallow fully connected network is shown in figure 3.4. The loss function is the mean squared error between predicted iEEG edge strength and its ground truth:

$$\mathcal{L}^{MSE} = ||Y - \hat{Y}||_2^2 = ||Y - f(X; W)||_2^2$$

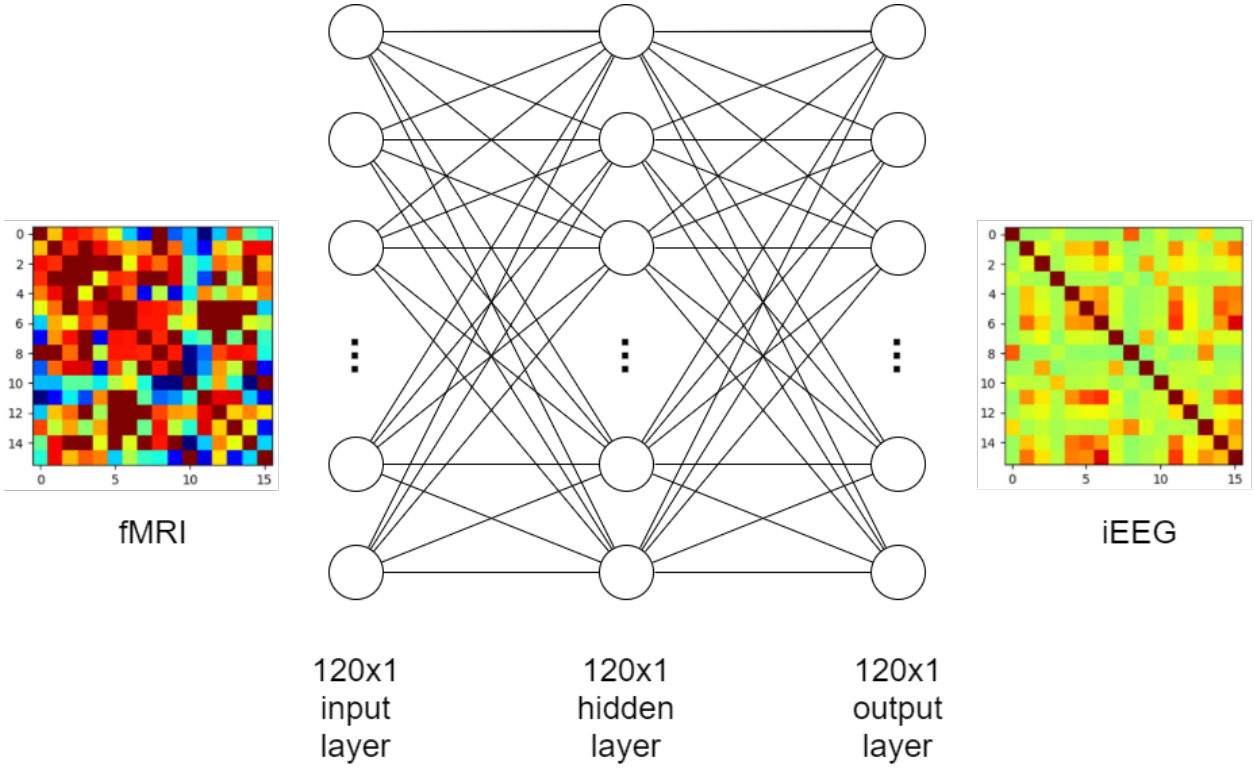

Figure 3.4: Shallow Fully Connected Network

where W is the set of weights in the deep neural network.

We used Leaky Rectifier Unit (ReLU) as activation function for each layer, where a leaky value of $x/3$ is set for $x < 0$ [KBM17]. We used Adam optimizer with learning rate 2e$-$4 to optimize the loss function, each weight update is done every batch of 3 if no permutation or 300 if there are 100 permutations. We train for 100 epochs with cross-validation and select the model having the lowest loss. Evaluation and hyperparameter tuning were done using 4-fold cross-validation, and the model yielding best validation loss is used to perform prediction on the testing set comprising data of 3 patients.

3.4.2 Encoder-Decoder Model

Our Encoder-Decoder model takes inspirations from Autoencoder architecture with multiple fully connected layers shrinking down the input to a compact representation at the bottleneck, then respring it back into the original dimension also by multiple fully connected layers.

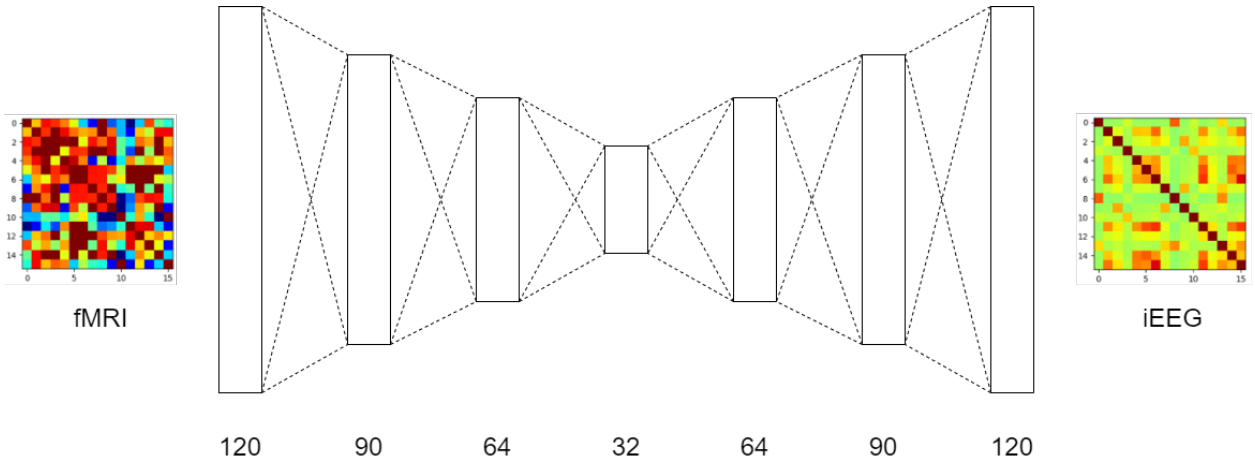

Figure 3.5: Encoder-Decoder Network

However, unlike autoencoder which is an unsupervised method (the target is also the input), we set the target to be vectorized iEEG connectivity matrix, and input to be vectorized fMRI connectivity matrix. This way the bottleneck layer can be interpreted as a compact representation of the fMRI input that optimizes the reconstruction of iEEG output. We design our encoder and decoder to have 3 layers each, in addition to the bottleneck layer. We chose the dimensions of encoder layers to be 120, 90, 64, respectively, and 64, 90, 120 for decoder. The size of the bottleneck layer is chosen to be 32. Figure 3.5 illustrates our encoder-decoder architecture. We used the same MSE loss function, Adam optimizer, Leaky ReLU activation, number of epochs and batch size as in the shallow fully connected network, and set learning rate to be 1e−4.

3.4.3 Double Autoencoder Model with Shared Latent Space

One of the benefits of using the above encoder-decoder model is having a compressed representation of the input that optimizes the reconstruction of the target. In the problem of cross-modality learning, a question arises as whether we can have a common representation of two modalities that can be used to reconstruct either one? In other words, how can we make a bidirectional cross-modality model that can not only infer modal B from modal A but can also infer modal A from modal B? Some prior works have proposed a double-autoencoder architecture to achieve this goal. We take inspiration from [SSP18] to build our

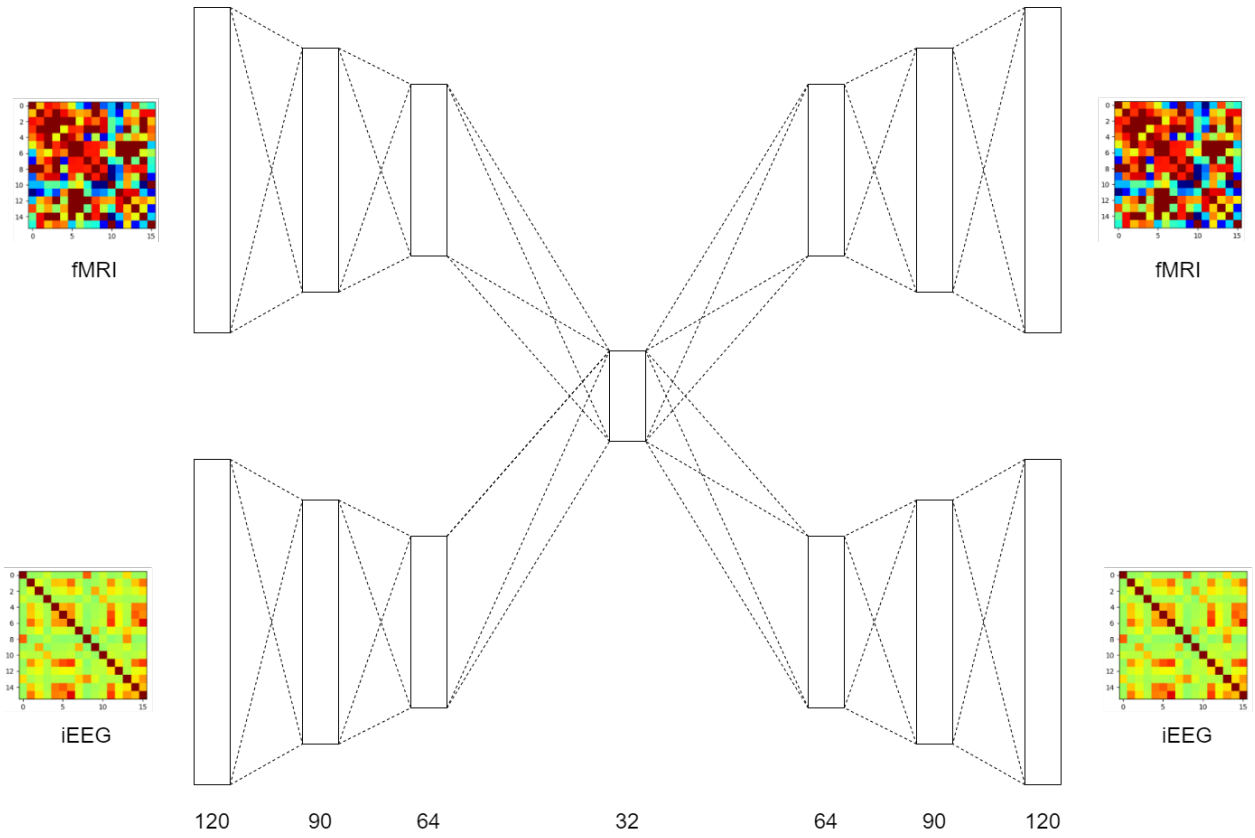

Figure 3.6: Double Autoencoder Model with Shared Latent Space

double autoencoder with shared latent space, as depicted in figure 3.6. The architecture basically consists of two encoder-decoder network that were presented in the previous section. These two networks would share a common bottleneck layer in the middle. Either fMRI input or iEEG input is fed to the network at a time, and the network will output either the reconstructed input or the target output of the other modality. Thus, only one pair of encoder-decoder is active at one pass. The four encoder-decoder pairs will take turn to be active one after the other. The training algorithm is summarized in Algorithm 1.

For architecture implementation details, we used fully connected networks with ReLU activation for all layers. We keep batch size, number of permutations same as Shallow Fully Connected Network. We changed learning rate of Adam optimizer to $1e-4$, and trained for 200 epochs .

Algorithm 1: Double Autoencoder training algorithm

$\mathcal{P} = \{(f_{fMRI}, g_{fMRI}), (f_{fMRI}, g_{iEEG}), (f_{iEEG}, g_{fMRI}), (f_{iEEG}, g_{iEEG})\}$: pairs of encoder f and decoder g, where f_M encodes modality M to common space and g_M decodes from common space to modality M

$\mathcal{E}$: number of epochs.

$e \leftarrow 0$

while $e < \mathcal{E}$ **do**

  for $(f_M, g_N) \in \mathcal{P}$ **do**

    $(x_M, x_N) \leftarrow (X_M, X_N)$: sample data pair of modality M, N (M and N can be the same modality)

    $z \leftarrow f_M(x_M)$

    $\hat{x}_N \leftarrow g_N(z)$

    $\mathcal{L}^{MSE} = ||x_N - \hat{x}_N||_2^2$

    $\theta_{f_M} \leftarrow \theta_{f_M} - \nabla_{\theta_{f_M}}(\mathcal{L}^{MSE})$

    $\theta_{g_N} \leftarrow \theta_{g_N} - \nabla_{\theta_{g_N}}(\mathcal{L}^{MSE})$

  end

  $e \leftarrow e + 1$

end

3.4.4 U-BrainNet Model

One of the challenges working with connectomic data is that it is difficult to train a deep neural network (DNN) using the traditional methods. One way is to ignore the topology of the brain network and work on the vector of edge weights as input features. We can partially mitigate the effect of vectorized brain network on the isomorphic property of the network by introducing synthetic isomorphic inputs for the DNN to learn, as described in Problem Formulation section. However, it still does not solve the problem of throwing away complex relationship between edges in the brain network. In addition, fully connected network that is used in this way also has its limited learning capacity.

Another way is to treat the connectivity matrix as an image and apply convolution operation on the image, as how CNN does. However, traditional grid-like convolution operation, which is originally intended to extract spatial features on a rectangular local patch of the image, does not make sense when applied on connectivity matrix where adjacent rows and columns are independent to each other. Relationship between edges exist only within the same row or column, as those are the edges incident on the same vertex. Taking convolution of, say a 3x3 patch of the connectivity matrix, would not intuitively extract meaningful information. To tackle this challenge, Kawahara et al [KBM17] proposed BrainNetCNN architecture with special convolution operations: edge-to-edge, edge-to-node, node-to-graph, designed specifically for connectomic data. We will present their approach and describe how we take inspiration from these to design our custom U-BranNet model.

Definition 3.6. (Edge-to-edge layer) Given a feature map of a weighted brain network $G = \{A, \Omega\}$ where Ω is the set of vertices (ROIs) and $A \in \mathbb{R}^{|\Omega| x |\Omega|}$ is the connectivity matrix representing weights of all edges among the vertices, we have the output of the Edge-to-edge layer defined as follows:

$$\hat{A}_{ij} = \sum_{k}^{|\Omega|} (r_k A_{ik} + c_k A_{kj})$$

where $[r_k, c_k] = w \in \mathbb{R}^{2|\Omega|}$ is the filter weights.

The convolution process is visualized in Figure 3.7 where we can see a step-by-step

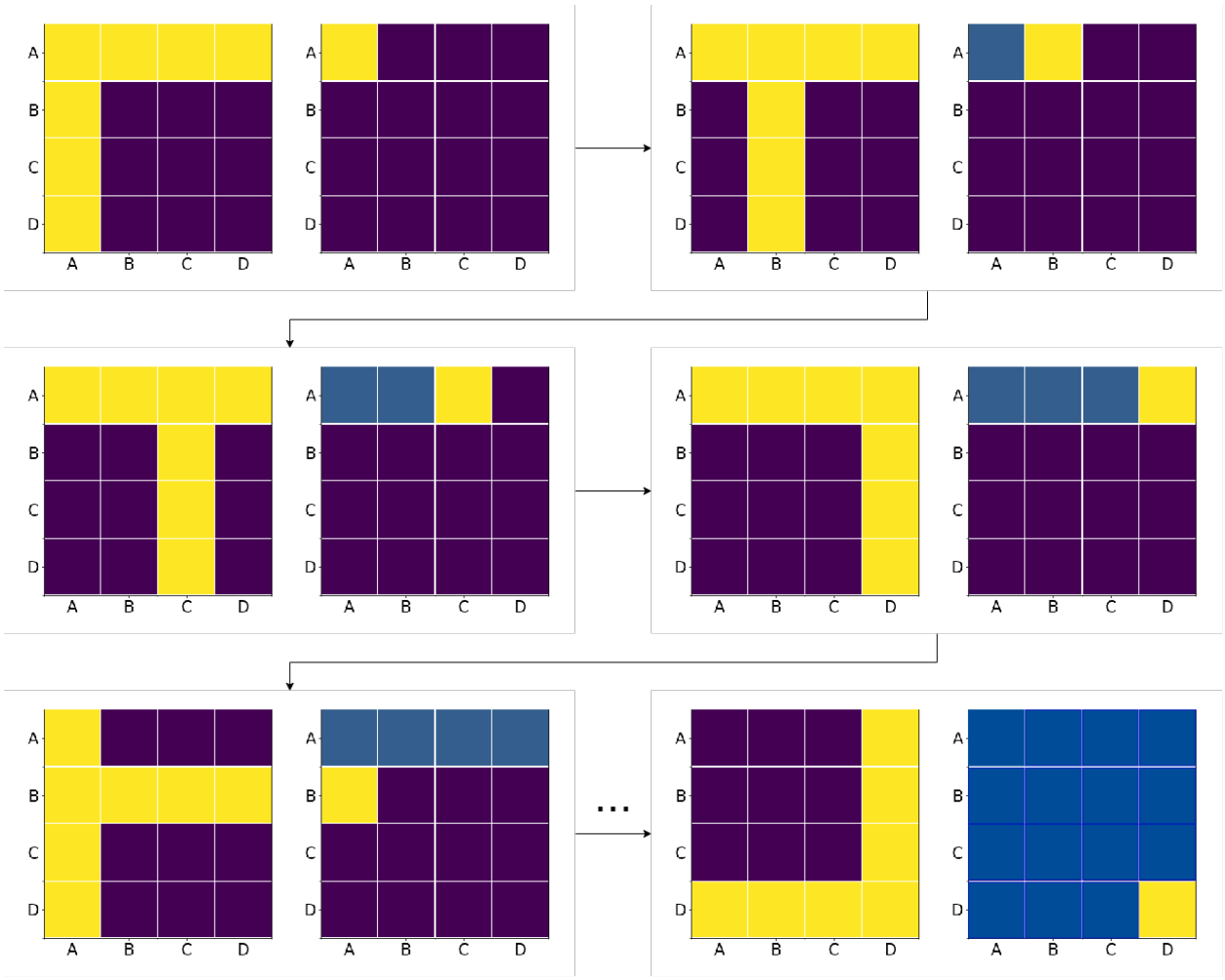

Figure 3.7: Visualization of edge-to-edge operation on one 4x4 feature map [KBM17]

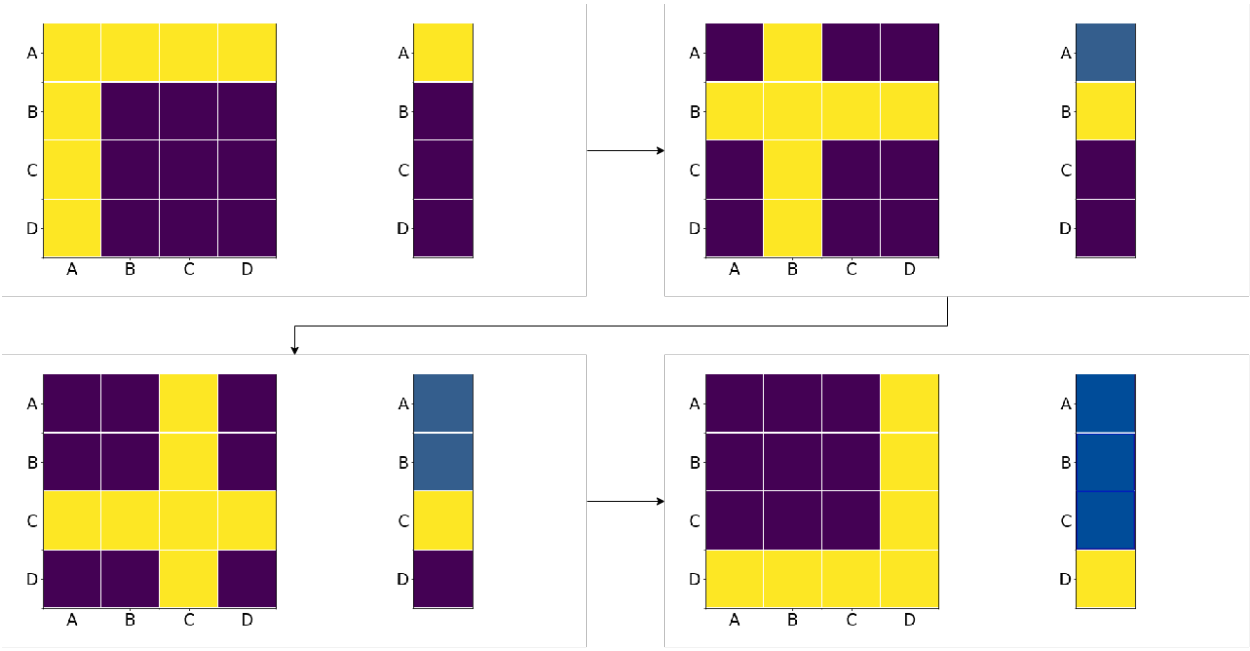

Figure 3.8: Visualization of edge-to-node operation on one 4x4 feature map [KBM17]

operation on a 4x4 feature map. The convolution filter here does not have a rectangular shape as in traditional CNN, but instead has a L, T or + shapes. It characterizes an edge by summarizing information across all edges incident on its two vertices. For further intuition behind the edge-to-edge convolution operation, refer to [KBM17]. Note that even if the input is a symmetric connectivity matrix, the resulting output may not be symmetric, as the filter weights are initialized randomly. However, it can be perceived as learning two separate feature maps, one from the upper triangle part of the matrix and one from the lower triangle [KBM17]. The edge-to-edge filter can be effectively implemented in Pytorch as the sum of two convolution outputs done by a Dx1 filter and a 1xD filter. This is in fact two built-in Conv2D layers in Pytorch with filters of size Dx1 and 1xD. We also note that since edge-to-edge convolution does not use padding, the output feature map has the same dimension as the input feature map.

Definition 3.7. (Edge-to-node layer) Given a feature map of a weighted brain network $G = \{A, \Omega\}$ where Ω is the set of vertices (ROIs) and $A \in \mathbb{R}^{|\Omega| \text{x} |\Omega|}$ is the connectivity matrix representing weights of all edges among the vertices, we have the output of the Edge-to-node

layer defined as follows:

$$\hat{a}_i = \sum_{k}^{|\Omega|} (r_k A_{ik} + c_k A_{ki})$$

where $[r_k, c_k] = w \in \mathbb{R}^{2|\Omega|}$ is the filter weights.

Remark 3.3. *Note that the output of edge-to-node layer is a D-by-1 vector, while output of edge-to-edge layer is a D-by-D matrix*

The convolution process is visualized in Figure 3.8 where we can see a step-by-step operation on a 4x4 feature map. It summarizes the information of all edges incident on one vertex to represent that vertex in the output vector. Edge-to-node operation can be implemented in PyTorch by a Conv2D layer with 1xD filter.

Definition 3.8. (Node-to-graph layer) Given a feature map of a weighted brain network $\mathrm{G} = \{A, \Omega\}$ where Ω is the set of vertices (ROIs) and $A \in \mathbb{R}^{|\Omega|\mathrm{x}|\Omega|}$ is the connectivity matrix representing weights of all edges among the vertices, we have the output of the Node-to-graph layer defined as follows:

$$\hat{a} = \sum_{k}^{|\Omega|} w_i a_i$$

where $w \in \mathbb{R}^{|\Omega|}$ is the filter weights.

Remark 3.4. *Note that the input of node-to-graph layer is the feature map output of edge-to-node layer, and output of node-to-graph layer is a scalar, while output of edge-to-edge layer is a D-by-D matrix, and output of edge-to-node layer is a D-by-1 matrix*

Node-to-graph layer summarizes the information of all vertices to a scalar representing the whole graph. Node-to-graph operation can be implemented in PyTorch by a Conv2D layer with Dx1 filter.

U-BrainNet model

Taking inspiration from U-Net [RFB15], whose architectures demonstrated an ability to extract a compact cross-modality representation of input data that optimizes its reconstruction of the target, and the efficient convolution operations applicable for connectomic data

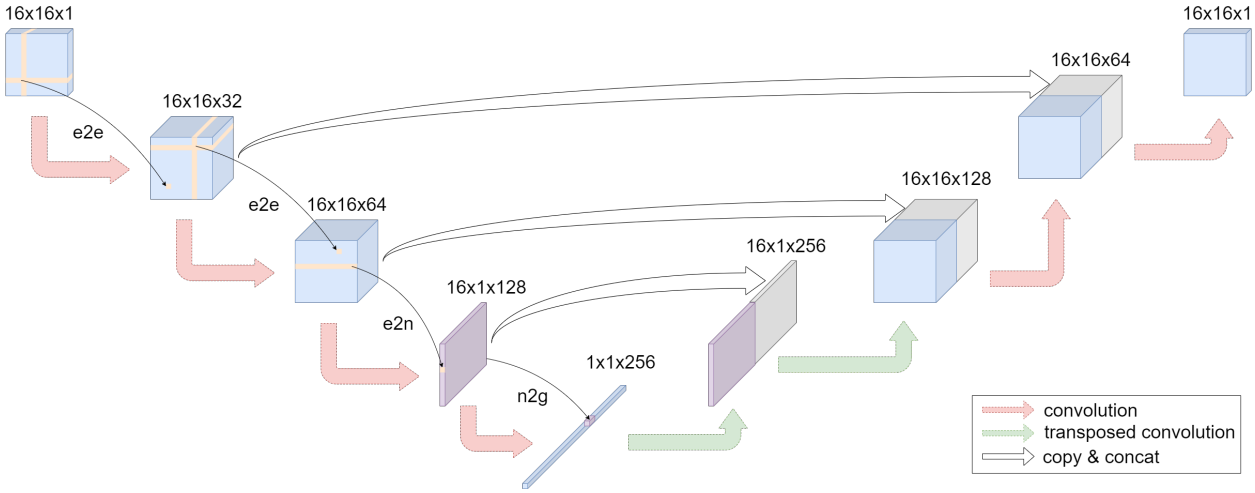

Figure 3.9: U-BrainNet

introduced by BrainNetCNN [KBM17], we proposed our custom model U-BrainNet. By U-BrainNet, we attempt to learn the abnormalities within the fMRI-derived epilepsy network and translate them to the iEEG-derived epilepsy network. iEEG-derived network certainly contains abnormalities of brain network, but in a form different from that of fMRI-derived network. We note that this thesis does not try to interpret the iEEG network abnormalities, but rather attempt to reconstruct it as accurate as possible and leave the interpretation to neurosurgeons and epilepsy experts. U-BrainNet comprised of an encoder and a decoder. The encoder is a sequence of two edge-to-edge convolution layers, followed by edge-to-node and node-to-graph layers. The bottleneck is the output of node-to-graph layer, which essentially is a compact representation of the whole graph. As layers get deeper, we increase the number of convolution filters to compensate for the reduction of feature map dimensions [KBM17]. The decoder of U-BrainNet is a sequence of two deconvolution layers (transposed convolution) and two edge-to-edge convolution layers. The transposed convolution is meant to restore the original dimension of the feature maps. Following the technique used in U-Net, we copy and concatenate the feature maps at each stage of encoder to the feature maps at the corresponding stage of decoder. The intuition is that the original feature map in the encoder would guide its reconstruction in the decoder [RFB15]. In the last two layers of decoder, we use the edge-to-edge convolution again instead of transposed convolution, since

there is no need for rematching feature map dimension. Certainly a transposed convolution using a 1x1 filter would work too, but empirically we observed a better performance using edge-to-edge layer compared to transposed convolution. Final output is the of the same dimension of the input connectivity matrix, however, it might not be symmetric since the operations along the network flow do not conserve symmetry of the feature map. Therefore we flatten the last feature map and add a fully connected with output size of 16 to represent the upper half of the connectivity matrix. The full connectivity matrix can be computed by mirroring the upper triangle to the lower triangle. The result is the final output where the loss is computed. This way we have imposed the symmetric constraint on the reconstruction of the connectivity matrix. We used the same MSE loss function, Adam optimizer, ReLU activation, number of epochs and batch size as in the shallow fully connected network, and set learning rate to be 1e−5.

Appendix: Architectures of proposed deep learning models

ShallowNet:

ShallowNet(

(dense1): Linear(in_features=120, out_features=120, bias=True)

(dense2): Linear(in_features=120, out_features=120, bias=True)

(dense3): Linear(in_features=120, out_features=120, bias=True)

)

Encoder-Decoder:

Encoder-Decoder(

(fc1_1): Linear(in_features=120, out_features=90, bias=True)

(fc1_2): Linear(in_features=90, out_features=64, bias=True)

(fc1_3): Linear(in_features=64, out_features=32, bias=True)

(fc1_4): Linear(in_features=32, out_features=16, bias=True)

(fc2_1): Linear(in_features=16, out_features=32, bias=True)

(fc2_2): Linear(in_features=32, out_features=64, bias=True)

(fc2_3): Linear(in_features=64, out_features=90, bias=True)

(fc2_4): Linear(in_features=90, out_features=120, bias=True)

)

Double Autoencoder:

DoubleAutoencoder(

(fcAe1): Linear(in_features=120, out_features=90, bias=True)

(fcAe2): Linear(in_features=90, out_features=64, bias=True)

(fcAe3): Linear(in_features=64, out_features=32, bias=True)

(fcAe4): Linear(in_features=32, out_features=16, bias=True)

(fcBe1): Linear(in_features=120, out_features=90, bias=True)

(fcBe2): Linear(in_features=90, out_features=64, bias=True)

(fcBe3): Linear(in_features=64, out_features=32, bias=True)

(fcBe4): Linear(in_features=32, out_features=16, bias=True)

(fcAd1): Linear(in_features=16, out_features=32, bias=True)

(fcAd2): Linear(in_features=32, out_features=64, bias=True)

(fcAd3): Linear(in_features=64, out_features=90, bias=True)

(fcAd4): Linear(in_features=90, out_features=120, bias=True)

(fcBd1): Linear(in_features=16, out_features=32, bias=True)

(fcBd2): Linear(in_features=32, out_features=64, bias=True)

(fcBd3): Linear(in_features=64, out_features=90, bias=True)

(fcBd4): Linear(in_features=90, out_features=120, bias=True)

)

U-BrainNet:

BrainNetCNN(

(e2econv1): E2EBlock(

(cnn1): Conv2d(1, 32, kernel_size=(1, 16), stride=(1, 1))

(cnn2): Conv2d(1, 32, kernel_size=(16, 1), stride=(1, 1))

)

(e2econv2): E2EBlock(

(cnn1): Conv2d(32, 32, kernel_size=(1, 16), stride=(1, 1))

(cnn2): Conv2d(32, 32, kernel_size=(16, 1), stride=(1, 1))

)

(E2N): Conv2d(32, 64, kernel_size=(1, 16), stride=(1, 1))

(N2G): Conv2d(64, 256, kernel_size=(16, 1), stride=(1, 1))

(G2N): ConvTranspose2d(256, 64, kernel_size=(16, 1), stride=(1, 1))

(N2E): ConvTranspose2d(128, 32, kernel_size=(1, 16), stride=(1, 1))

(e2econv3): E2EBlock(

(cnn1): Conv2d(64, 32, kernel_size=(1, 16), stride=(1, 1))

(cnn2): Conv2d(64, 32, kernel_size=(16, 1), stride=(1, 1))

)

(e2econv4): E2EBlock(

(cnn1): Conv2d(64, 1, kernel_size=(1, 16), stride=(1, 1))

(cnn2): Conv2d(64, 1, kernel_size=(16, 1), stride=(1, 1))

)

(dense1): Linear(in_features=256, out_features=120, bias=True)

)

CHAPTER 4

Evaluation

4.1 Evaluation Metrics

Since our models try to predict real-valued edge strength in the iEEG-derived epilepsy network, we choose to report mean absolute error (MAE) between ground truth value and predicted value as an evaluation metrics. In addition to MAE, we also report the standard deviation of the squared error (SDAE) to measure the variability of the squared error. One problem with MAE is that it fails to measure the goodness of the prediction in cases where there is not much variability in the ground truth connectivity matrix [KBM17]. In those cases, a random prediction around the average of the ground truth would yield a low MAE, but certainly would not mean the model has learned sufficiently. We therefore also report the Pearson's correlation coefficients (r) between the ground truth and the prediction. If the prediction matches the ground truth perfectly, we will have a Pearson's correlation of 1. Pearson's correlation near zero means the prediction does not correlate with the ground truth. Negative Pearson's correlation means prediction is negatively correlated with ground truth. Pearson's correlation becomes a bad performance indicator, however, when the predictor constantly predicts too high above or too low below the $y = x$ line but still forms a distribution parallel to the $y = x$ line. MAE in that case would give a better insight. Therefore we choose to report both MAE and Pearson's correlation just as [KBM17]. We also report the associated p-value along with Pearson's correlation coefficient. p-value of an associated r is the probability that we find abs(r') of a sample X, Y drawn from a noncorrelated population to be greater or equal to abs(r). In other words, p-value signifies how statistically significant the r value is. Typically a p-value < 0.05 means the result is significant.

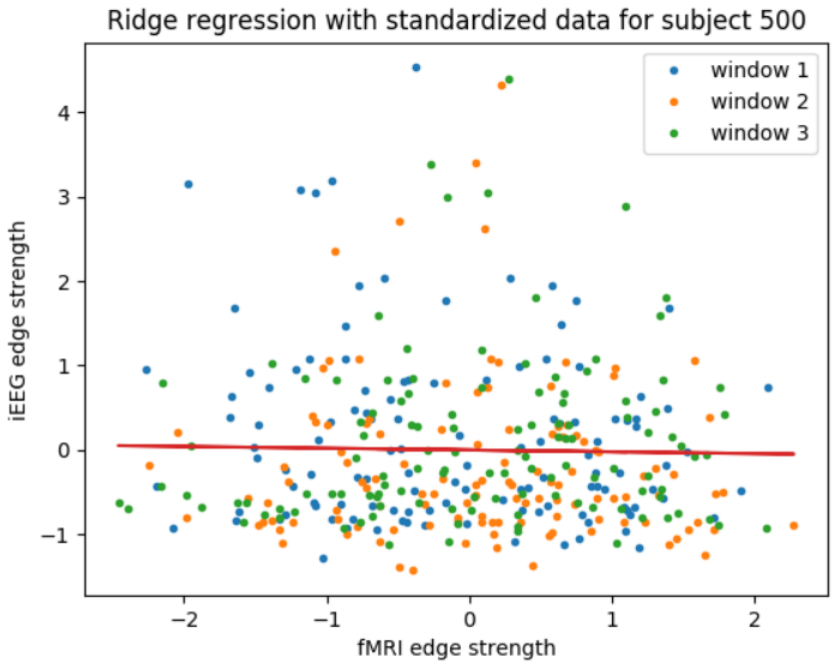

Figure 4.1: Ridge Regression on fMRI-iEEG edge strength

4.2 Evaluation of Pairwise Connectivity Level Prediction

We standardized the input and ran a Ridge regression with $\alpha = 1$ to predict the edge strength based on the assumption that the mapping between fMRI edge strength to iEEG edge strength happens individually and independently irrespective of what edge in the network we are predicting or any relationship existing among the edges. We plot the data distribution and the regression line in Figure 4.1 to visualize the result. As apparent from the plot, we did not observe a relationship between fMRI edge strength and iEEG edge strength. The regression line just predicted the average of the distribution. Therefore we conclude that the mapping between fMRI and iEEG edge strength does not happen based merely on the value of the edge strength. Other features such as the collective edge strengths of the whole network should be considered, since it is likely that the strength of a particular edge depends on the interaction with other edges in the network.

	Testing				Best Validation			
Model	MAE	SDAE	r	p	MAE	SDAE	r	p
ShallowNet	0.139	0.003	0.081	0.007	0.036	0.007	0.075	0.004
Encoder-Decoder	0.134	0.002	0.047	0.125	0.029	0.008	0.192	$< 1e{-5}$
Double Autoencoder	0.132	0.011	0.008	0.793	1.737	0.315	0.207	$< 1e{-5}$
U-BrainNet	0.127	0.128	0.021	0.479	0.030	0.009	0.113	$< 1e{-5}$

Table 4.1: Comparison of performance for proposed models.

4.3 Quantitative Evaluation of Connectome Level Prediction

For all deep learning model, we used Adam optimizer to optimize the loss function, each weight update is done every batch of 3 if no permutation or 300 if there are 100 permutations. We train for at least 100 epochs for all models. All models show lowest point of validation curve within the first 100 epochs. Evaluation and hyperparameter tuning were done using 4-fold cross-validation, and the model yielding best validation loss was used to perform prediction on the testing set comprising data of 3 patients. In Table 4.3, we compare the performance of four proposed models on the testing set. We note that for Double Autoencoder, validation loss was calculated by summing losses incurred by 4 pairs of encoder-decoder in 4 passes, rather than a straightforward pass in other three models, thus its MAE numerical value is high compared to other models. However, testing MAE of Double Autoencoder was done using the fMRI-iEEG encoder-decoder pair only, thus its numerical value is on the same scale with other three models.

We observed that even though U-BrainNet (the most sophisticated model) gives the lowest testing MAE, its Pearson's correlation coefficient is small and p-value hints that this prediction is not statisticaly significant. We observed the same insignificance in the other three models. When the Pearson's correlation coefficient is around zero, MAE does not bear much meaning. This bad performance on testing data happened despite the relatively good performance (both in terms of MAE and Pearson's correlation) on validation data. We will give some of our reasoning behind these results in the chapter 5 (Discussion). We show a

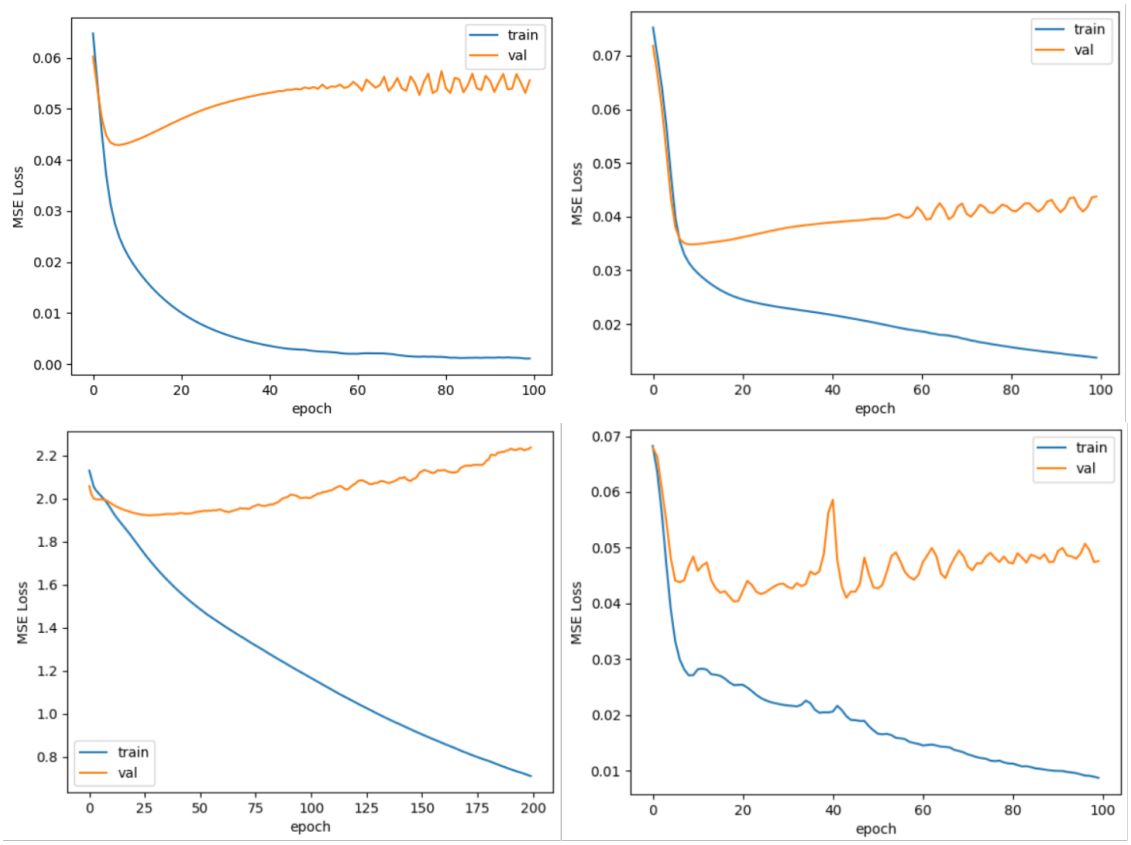

Figure 4.2: Training and validation losses over the course of training. From left to right, top to bottom: ShallowNet, Encoder-Decoder, Double Autoencoder, U-BrainNet.

training and validation curves in Figure 4.2 to have a closer look into the training process. As can be seen from the plots, the proposed models were able to overfit the training dataset. However, the best validation loss stays relatively similar around 0.04 for all models (except Double Autoencoder where the validation loss is summed across 4 passes of alternating encoder-decoder pairs thus is not on the same scale with the other three models). We also tested the models with permuted input connectivity matrices, but saw a worse performance (results not shown here). It hints that the data may have reached its noise level that any improvements on the model would not give a better validation, and adding more (bad) data by permuting the input matrices would not help the models learn better.

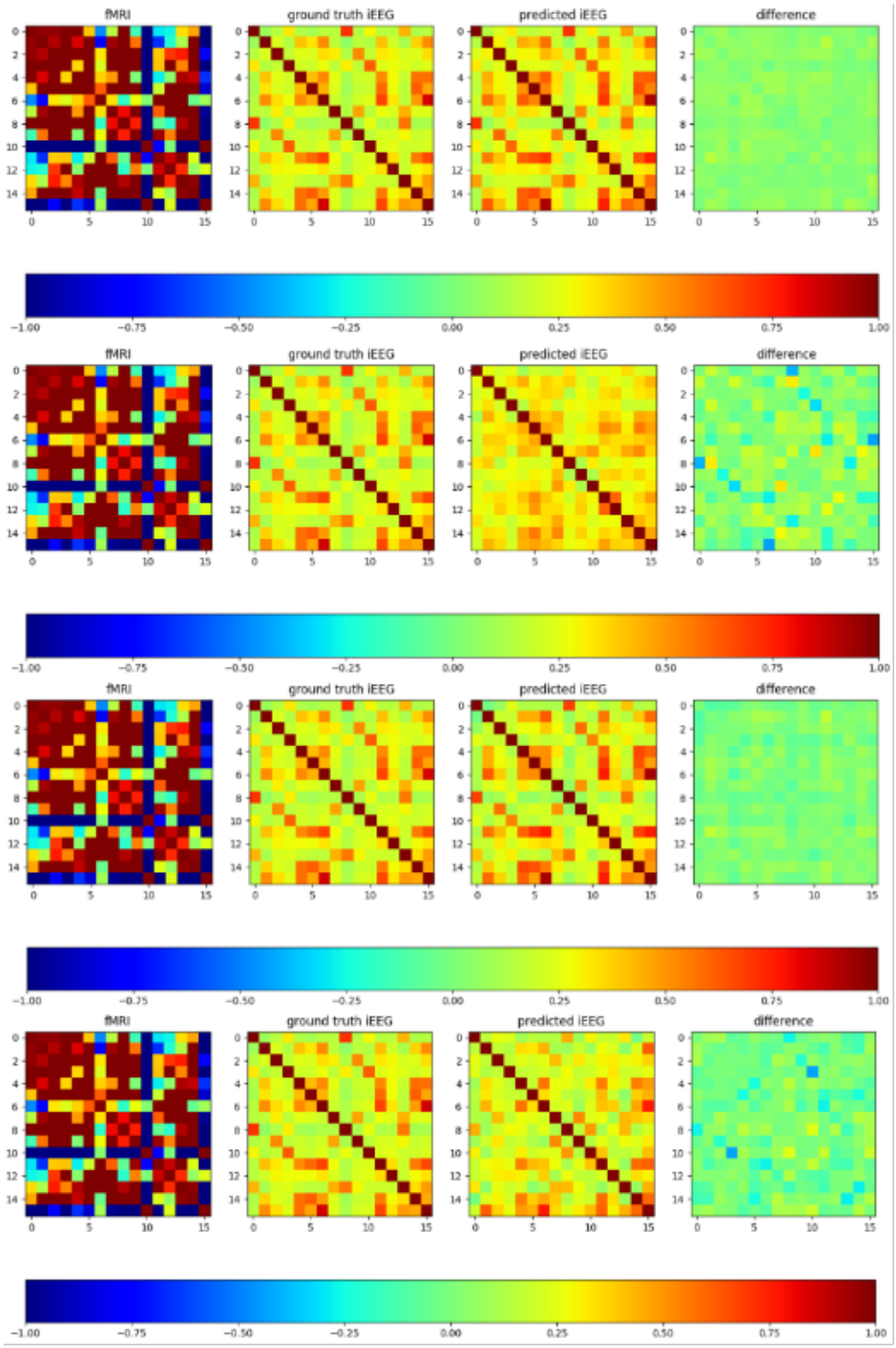

Figure 4.3: Prediction of models on training samples. From top to bottom: ShallowNet, Encoder-Decoder, Double Autoencoder, U-BrainNet.

4.4 Qualitative Evaluation of Connectome Level Prediction

In this section we will visualize some prediction of the four proposed models on some training and testing samples. For training samples we show the prediction at the last epoch (the end of training), showing how the models overfit training data (Figure 4.3). For testing samples we show the prediction by the model having best validation error (Figure 4.4). All four models were able to overfit the training set as they reconstructed the iEEG connectivity matrix nearly identical to the ground truth. The reconstruction on the testing set, however, was not as good. Most of the time the reconstruction did not capture the prominent elements (highly correlated edges) in the iEEG network.

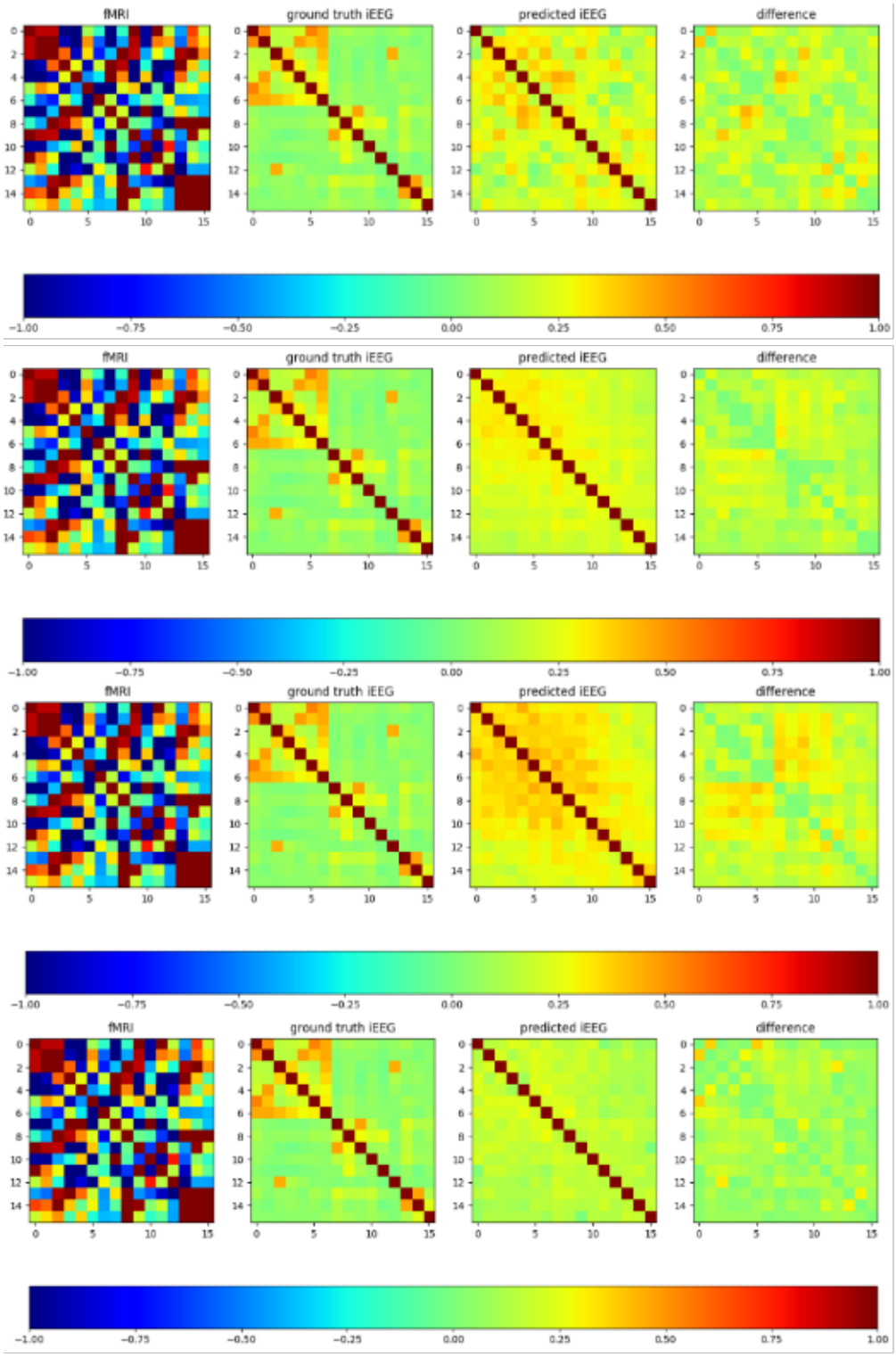

Figure 4.4: Prediction of models on testing samples. From top to bottom: ShallowNet, Encoder-Decoder, Double Autoencoder, U-BrainNet.

CHAPTER 5

Discussion and Future Work

Although the best performance on the validation set was relatively good, and we used the model that obtained this best validation to perform prediction on the testing set, the testing results were not as good. It can be seen from Table 4.3 that the prediction does not correlate well with ground truth values, hinting that the models were not able to generalize new unseen testing samples. There might be some reasons for this dire performance.

Hyperparameter tuning is insufficient? Although we tried our best to optimize hyperparameters for each model, there is still a chance that we did not discover the range of optimal ones that yield reasonable statistical significance. In future work we might continue to further optimize the proposed models by a hyperparameter grid-search.

Current training set is not large enough for model to generalize? It could be that we did not have training data large enough for the model to learn effectively (we analyzed 43 subjects, among which 3 subjects are reserved for testing). This is a typical problem for medical data, where obtaining large sample size is often difficult. When trained on a limited set, the sophisticated features characterizing brain network abnormalities are not sufficiently represented by the set, resulting in model high variance.

Model prediction capacity has reached the noise limitation of fMRI data? The resting state fMRI time series signal is infamously noisy. Plus, due to limitation in clinical recording sessions, a session lasts only 4-8 minutes, and only one scan is taken every 2 seconds. This fact leaves us with relatively large variability among the extracted windows (refer to prior section of fMRI preprocessing for further details). This, coupled with the fact that resting state fMRI's large variability (we cannot control what subjects think during the scanning session, which would result in noisy hemodynamic activities distorting our data),

leads to bad data and confused the neural network. This might explain why when we feed permuted versions of (already noisy) connectivity matrices to the neural networks, we did not observe improved prediction. Further improvements on data acquisition and preprocessing techniques are needed to reduce the variability in the fMRI. Approaches may include better controlled recording protocol and using longer sliding windows to sufficiently reduce the noise level within the window.

Limited sampling of iEEG hinders characterization of epileptic network? In this work, due to limited spatial sampling of iEEG, we only perform prediction on a 16x16 connectivity matrix, as 16 is the minimum number of ROIs having electrodes implanted on one patient. It is possible that an epileptic network can only be fully characterize on a larger scale, i.e. with more vertices and edges. Limited sampling of iEEG electrodes is an unavoidable problem for this type of study. However, we can make the most out of available data by not discarding excessive data in patients having more than 16 ROIs. The technical issue preventing us to do so is that our neural network architectures can only handle fixed input size, thus we need to sync this dimension for all patients. Advanced neural network methods such as graph neural network may solve this issue since it can handle variable input graph sizes thus will be part of our future work. These approaches may also open opportunities for using the whole brain network of fMRI for prediction, which is one of the benefits offered by fMRI that iEEG does not have.

Assumption on the current cross-modality relationship is not valid? It is possible that there is inherently no correlation between the fMRI and iEEG features that we used. Currently we compute correlation of signals between ROIs as edge strengths. The signal was first filtered at low frequency range 0.01-0.1Hz for fMRI (typical frequency used in the literature for resting state fMRI), and low gamma band for iEEG. This does not rule out the possibility that there is a correlation between fMRI and iEEG networks at other frequency bands, or between features other than Pearson's correlation, such as gamma event coupling or other graph measures [MKD15]. We leave this exploration to our future work.

CHAPTER 6

Conclusion

In this thesis we explored the feasibility of bridging the gap across fMRI-derived epileptic network and iEEG-derived epileptic network. The study if successful will equip us with a computational tool to construct iEEG network - a gold standard in epilepsy analysis - without the need for risky surgery procedures. We proposed a data-driven approach and presented four deep neural network models to tackle this cross-modality challenge. Our most sophisticated model - U-BrainNet - was designed with architectural consideration specifically targeting connectomic data and cross-modality learning. fMRI and iEEG data was obtained from 43 patients with intractable epilepsy. We perform a 4-fold cross-validation and used the best model to evaluate testing set. The best performance across the models currently has not reached a level to become clinically reliable. We offered some insights into the current challenges and proposed multiple future approaches to tackle these issues.

REFERENCES

[AAW15] Samuel Ahn, Catalina Alvarado-Rojas, Shennan Weiss, Anatol Bragin, Richard Staba, and Jerome Engel. "Gamma Event Functional Connectivity (GEFC) and Graph Theory Measures in Mesial Temporal Lobe Epilepsy: S302." *Annals of Neurology*, **78**, 2015.

[Aka06] Shotaro Akaho. "A kernel method for canonical correlation analysis." *arXiv preprint cs/0609071*, 2006.

[AMS14] Ishmael Amarreh, Mary E Meyerand, Carl Stafstrom, Bruce P Hermann, and Rasmus M Birn. "Individual classification of children with epilepsy using support vector machine with multiple indices of diffusion tensor imaging." *NeuroImage: Clinical*, **4**:757–764, 2014.

[BLW17] Fabrice Bartolomei, Stanislas Lagarde, Fabrice Wendling, Aileen McGonigal, Viktor Jirsa, Maxime Guye, and Christian Bénar. "Defining epileptogenic networks: contribution of SEEG and signal analysis." *Epilepsia*, **58**(7):1131–1147, 2017.

[BMR19] Alaa Bessadok, Mohamed Ali Mahjoub, and Islem Rekik. "Symmetric Dual Adversarial Connectomic Domain Alignment for Predicting Isomorphic Brain Graph from a Baseline Graph." In *International Conference on Medical Image Computing and Computer-Assisted Intervention*, pp. 465–474. Springer, 2019.

[BPP17] Alejandro O Blenkmann, Holly N Phillips, Juan P Princich, James B Rowe, Tristan A Bekinschtein, Carlos H Muravchik, and Silvia Kochen. "iElectrodes: a comprehensive open-source toolbox for depth and subdural grid electrode localization." *Frontiers in neuroinformatics*, **11**:14, 2017.

[BTB65] Jean Bancaud, Jean Talairach, A Bonis, C Schaub, G Szikla, P Morel, and M Bordas-Ferrer. "La stéreoencephalographie dans l'épilepsie." *Mattson, Paris*, pp. 113–146, 1965.

[BWE00] A Bragin, CL Wilson, and J Engel Jr. "Chronic epileptogenesis requires development of a network of pathologically interconnected neuron clusters: a hypothesis." *Epilepsia*, **41**:S144–S152, 2000.

[CAV16] Lluis Castrejon, Yusuf Aytar, Carl Vondrick, Hamed Pirsiavash, and Antonio Torralba. "Learning aligned cross-modal representations from weakly aligned data." In *Proceedings of the IEEE Conference on Computer Vision and Pattern Recognition*, pp. 2940–2949, 2016.

[CCG16] Sharon Chiang, Alberto Cassese, Michele Guindani, Marina Vannucci, Hsiang J Yeh, Zulfi Haneef, and John M Stern. "Time-dependence of graph theory metrics in functional connectivity analysis." *NeuroImage*, **125**:601–615, 2016.

[DBP11] Jane De Tisi, Gail S Bell, Janet L Peacock, Andrew W McEvoy, William FJ Harkness, Josemir W Sander, and John S Duncan. "The long-term outcome of

adult epilepsy surgery, patterns of seizure remission, and relapse: a cohort study." *The Lancet*, **378**(9800):1388–1395, 2011.

[DDS09] Jia Deng, Wei Dong, Richard Socher, Li-Jia Li, Kai Li, and Li Fei-Fei. "Imagenet: A large-scale hierarchical image database." In *2009 IEEE conference on computer vision and pattern recognition*, pp. 248–255. Ieee, 2009.

[DWK16] John S Duncan, Gavin P Winston, Matthias J Koepp, and Sebastien Ourselin. "Brain imaging in the assessment for epilepsy surgery." *The Lancet Neurology*, **15**(4):420–433, 2016.

[ETS13] Jerome Engel Jr, Paul M Thompson, John M Stern, Richard J Staba, Anatol Bragin, and Istvan Mody. "Connectomics and epilepsy." *Current opinion in neurology*, **26**(2):186, 2013.

[EYM17] Bahareh Elahian, Mohammed Yeasin, Basanagoud Mudigoudar, James W Wheless, and Abbas Babajani-Feremi. "Identifying seizure onset zone from electrocorticographic recordings: a machine learning approach based on phase locking value." *Seizure*, **51**:35–42, 2017.

[FHH16] Paul Fergus, A Hussain, David Hignett, Dhiya Al-Jumeily, Khaled Abdel-Aziz, and Hani Hamdan. "A machine learning system for automated whole-brain seizure detection." *Applied Computing and Informatics*, **12**(1):70–89, 2016.

[GE01] J Girvin and M Eliasziw. "Effectiveness and Efficiency of Surgery for Temporal Lobe Epilepsy Study Group. A randomized, controlled trial of surgery for temporal-lobe epilepsy." *N Engl J Med*, **345**(5):3l, 2001.

[Glo11] Gary H Glover. "Overview of functional magnetic resonance imaging." *Neurosurgery Clinics*, **22**(2):133–139, 2011.

[GMB18] Ezequiel Gleichgerrcht, Brent Munsell, Sonal Bhatia, William A Vandergrift III, Chris Rorden, Carrie McDonald, Jonathan Edwards, Ruben Kuzniecky, and Leonardo Bonilha. "Deep learning applied to whole-brain connectome to determine seizure control after epilepsy surgery." *Epilepsia*, **59**(9):1643–1654, 2018.

[GWX19] Yunhao Ge, Dongming Wei, Zhong Xue, Qian Wang, Xiang Zhou, Yiqiang Zhan, and Shu Liao. "Unpaired Mr to CT Synthesis with Explicit Structural Constrained Adversarial Learning." In *2019 IEEE 16th International Symposium on Biomedical Imaging (ISBI 2019)*, pp. 1096–1099. IEEE, 2019.

[Han17] Xiao Han. "MR-based synthetic CT generation using a deep convolutional neural network method." *Medical physics*, **44**(4):1408–1419, 2017.

[HAZ18] Rasoul Hekmati, Robert Azencott, Wei Zhang, Zili D Chu, and Michael J Paldino. "Localization of Epileptic Seizure Focus by Computerized Analysis of fMRI Recordings." *arXiv preprint arXiv:1812.04533*, 2018.

[HCY15] Zulfi Haneef, Sharon Chiang, Hsiang J Yeh, Jerome Engel Jr, and John M Stern. "Functional connectivity homogeneity correlates with duration of temporal lobe epilepsy." *Epilepsy & Behavior*, **46**:227–233, 2015.

[HLY14] Zulfi Haneef, Agatha Lenartowicz, Hsiang J Yeh, Harvey S Levin, Jerome Engel Jr, and John M Stern. "Functional connectivity of hippocampal networks in temporal lobe epilepsy." *Epilepsia*, **55**(1):137–145, 2014.

[HSS04] David R Hardoon, Sandor Szedmak, and John Shawe-Taylor. "Canonical correlation analysis: An overview with application to learning methods." *Neural computation*, **16**(12):2639–2664, 2004.

[HTP17] Mohammad-Parsa Hosseini, Tuyen X Tran, Dario Pompili, Kost Elisevich, and Hamid Soltanian-Zadeh. "Deep learning with edge computing for localization of epileptogenicity using multimodal rs-fMRI and EEG big data." In *2017 IEEE International Conference on Autonomic Computing (ICAC)*, pp. 83–92. IEEE, 2017.

[HZP19] Peng Hu, Liangli Zhen, Dezhong Peng, and Pei Liu. "Scalable deep multimodal learning for cross-modal retrieval." In *Proceedings of the 42nd International ACM SIGIR Conference on Research and Development in Information Retrieval*, pp. 635–644, 2019.

[IFT12] Matthias Ihle, Hinnerk Feldwisch-Drentrup, César A Teixeira, Adrien Witon, Björn Schelter, Jens Timmer, and Andreas Schulze-Bonhage. "EPILEPSIAE–A European epilepsy database." *Computer methods and programs in biomedicine*, **106**(3):127–138, 2012.

[IZZ17] Phillip Isola, Jun-Yan Zhu, Tinghui Zhou, and Alexei A Efros. "Image-to-image translation with conditional adversarial networks." In *Proceedings of the IEEE conference on computer vision and pattern recognition*, pp. 1125–1134, 2017.

[JBB12] Mark Jenkinson, Christian F Beckmann, Timothy EJ Behrens, Mark W Woolrich, and Stephen M Smith. "Fsl." *Neuroimage*, **62**(2):782–790, 2012.

[JHL17] Ronghui Ju, Chenhui Hu, Quanzheng Li, et al. "Early diagnosis of Alzheimer's disease based on resting-state brain networks and deep learning." *IEEE/ACM transactions on computational biology and bioinformatics*, **16**(1):244–257, 2017.

[JHT19] Jue Jiang, Yu-Chi Hu, Neelam Tyagi, Pengpeng Zhang, Andreas Rimner, Joseph O Deasy, and Harini Veeraraghavan. "Cross-modality (CT-MRI) prior augmented deep learning for robust lung tumor segmentation from small MR datasets." *Medical physics*, **46**(10):4392–4404, 2019.

[JLC19] Dae Ung Jo, ByeongJu Lee, Jongwon Choi, Haanju Yoo, and Jin Young Choi. "Cross-modal Variational Auto-encoder with Distributed Latent Spaces and Associators." *arXiv preprint arXiv:1905.12867*, 2019.

[KBM17] Jeremy Kawahara, Colin J Brown, Steven P Miller, Brian G Booth, Vann Chau, Ruth E Grunau, Jill G Zwicker, and Ghassan Hamarneh. "BrainNetCNN: Convolutional neural networks for brain networks; towards predicting neurodevelopment." *NeuroImage*, **146**:1038–1049, 2017.

[KCS16] Junghoe Kim, Vince D Calhoun, Eunsoo Shim, and Jong-Hwan Lee. "Deep neural network with weight sparsity control and pre-training extracts hierarchical features and enhances classification performance: Evidence from whole-brain resting-state functional connectivity patterns of schizophrenia." *Neuroimage*, **124**:127–146, 2016.

[KH20] Cho Kyung-Ok and Jang Hyun-Jong. "Comparison of different input modalities and network structures for deep learning-based seizure detection." *Scientific Reports (Nature Publisher Group)*, **10**(1), 2020.

[KHE17] Hui Ming Khoo, Yongfu Hao, Nicolás von Ellenrieder, Natalja Zazubovits, Jeffery Hall, André Olivier, François Dubeau, and Jean Gotman. "The hemodynamic response to interictal epileptic discharges localizes the seizure-onset zone." *Epilepsia*, **58**(5):811–823, 2017.

[KKS17] Ryohei Kuga, Asako Kanezaki, Masaki Samejima, Yusuke Sugano, and Yasuyuki Matsushita. "Multi-task learning using multi-modal encoder-decoder networks with shared skip connections." In *Proceedings of the IEEE International Conference on Computer Vision Workshops*, pp. 403–411, 2017.

[Laz] Emanuel Lazar. "Graph Isomorphism.".

[LBH15] Yann LeCun, Yoshua Bengio, and Geoffrey Hinton. "Deep learning." *nature*, **521**(7553):436–444, 2015.

[LC01] H. Lüders and Y.G. Comair. *Epilepsy Surgery*. Lippincott Williams & Wilkins, 2001.

[MBB07] Kevin Murphy, Jerzy Bodurka, and Peter A Bandettini. "How long to scan? The relationship between fMRI temporal signal to noise ratio and necessary scan duration." *Neuroimage*, **34**(2):565–574, 2007.

[MBV17] Regina J Meszlényi, Krisztian Buza, and Zoltán Vidnyánszky. "Resting state fMRI functional connectivity-based classification using a convolutional neural network architecture." *Frontiers in neuroinformatics*, **11**:61, 2017.

[MKD15] Negar Memarian, Sally Kim, Sandra Dewar, Jerome Engel Jr, and Richard J Staba. "Multimodal data and machine learning for surgery outcome prediction in complicated cases of mesial temporal lobe epilepsy." *Computers in biology and medicine*, **64**:67–78, 2015.

[MZC17] Md Mursalin, Yuan Zhang, Yuehui Chen, and Nitesh V Chawla. "Automated epileptic seizure detection using improved correlation-based feature selection with random forest classifier." *Neurocomputing*, **241**:204–214, 2017.

[NSN18] Yasunori Nagahama, Alan J Schmitt, Daichi Nakagawa, Adam S Vesole, Janina Kamm, Christopher K Kovach, David Hasan, Mark Granner, Brian J Dlouhy, Matthew A Howard, et al. "Intracranial EEG for seizure focus localization: evolving techniques, outcomes, complications, and utility of combining surface and depth electrodes." *Journal of neurosurgery*, **1**(aop):1–13, 2018.

[NSS18] Ida A Nissen, Cornelis J Stam, Elisabeth CW van Straaten, Viktor Wottschel, Jaap C Reijneveld, Johannes C Baayen, Philip C de Witt Hamer, Sander Idema, Demetrios N Velis, and Arjan Hillebrand. "Localization of the epileptogenic zone using interictal MEG and machine learning in a large cohort of drug-resistant epilepsy patients." *Frontiers in neurology*, **9**:647, 2018.

[PHZ17] Yuxin Peng, Xin Huang, and Yunzhen Zhao. "An overview of cross-media retrieval: Concepts, methodologies, benchmarks, and challenges." *IEEE Transactions on circuits and systems for video technology*, **28**(9):2372–2385, 2017.

[PK18] Josef Parvizi and Sabine Kastner. "Human intracranial EEG: promises and limitations." *Nature neuroscience*, **21**(4):474, 2018.

[PMS14] Francesca Pittau, Pierre Mégevand, Laurent Sheybani, Eugenio Abela, Frédéric Grouiller, Laurent Spinelli, Christoph M Michel, Margitta Seeck, and Serge Vulliemoz. "Mapping epileptic activity: sources or networks for the clinicians?" *Frontiers in neurology*, **5**:218, 2014.

[RAY16] Scott Reed, Zeynep Akata, Xinchen Yan, Lajanugen Logeswaran, Bernt Schiele, and Honglak Lee. "Generative adversarial text to image synthesis." *arXiv preprint arXiv:1605.05396*, 2016.

[RFB15] Olaf Ronneberger, Philipp Fischer, and Thomas Brox. "U-net: Convolutional networks for biomedical image segmentation." In *International Conference on Medical image computing and computer-assisted intervention*, pp. 234–241. Springer, 2015.

[Ruo13] K Ruohonen. "Graph theory, Graafiteoria lecture notes, TUT.", 2013.

[SDK17] Nishant Sinha, Justin Dauwels, Marcus Kaiser, Sydney S Cash, M Brandon Westover, Yujiang Wang, and Peter N Taylor. "Predicting neurosurgical outcomes in focal epilepsy patients using computational modelling." *Brain*, **140**(2):319–332, 2017.

[SLS11] Steven M Stufflebeam, Hesheng Liu, Jorge Sepulcre, Naoaki Tanaka, Randy L Buckner, and Joseph R Madsen. "Localization of focal epileptic discharges using functional connectivity magnetic resonance imaging." *Journal of neurosurgery*, **114**(6):1693–1697, 2011.

[Smi02] Stephen M Smith. "Fast robust automated brain extraction." *Human brain mapping*, **17**(3):143–155, 2002.

[SSP18] Adrian Spurr, Jie Song, Seonwook Park, and Otmar Hilliges. "Cross-modal deep variational hand pose estimation." In *Proceedings of the IEEE Conference on Computer Vision and Pattern Recognition*, pp. 89–98, 2018.

[Sta14] Cornelis J Stam. "Modern network science of neurological disorders." *Nature Reviews Neuroscience*, **15**(10):683–695, 2014.

[STP13] Xilin Shen, Fuyuze Tokoglu, Xenios Papademetris, and R Todd Constable. "Groupwise whole-brain parcellation from resting-state fMRI data for network node identification." *Neuroimage*, **82**:403–415, 2013.

[SZC20] Zengming Shen, S Kevin Zhou, Yifan Chen, Bogdan Georgescu, Xuqi Liu, and Thomas Huang. "One-to-one Mapping for Unpaired Image-to-image Translation." In *The IEEE Winter Conference on Applications of Computer Vision*, pp. 1170–1179, 2020.

[SZY20] Yue Shi, Xin Zhang, Chunlan Yang, Jiechuan Ren, Zhimei Li, and Qun Wang. "A review on epileptic foci localization using resting-state functional magnetic resonance imaging." *Mathematical Biosciences and Engineering*, **17**(3):2496, 2020.

[Tib] Ryan Tibshirani. "Modern Regression 1: Ridge Regression.".

[TMP17] Samuel Tomlinson, Eric Marsh, and Brenda Porter. "Interictal network synchrony and local heterogeneity predict seizure relief following pediatric epilepsy surgery (S55. 001).", 2017.

[UCD07] Elena Urrestarazu, Rahul Chander, Francçois Dubeau, and Jean Gotman. "Interictal high-frequency oscillations (100–500 Hz) in the intracerebral EEG of epileptic patients." *Brain*, **130**(9):2354–2366, 2007.

[Udd13] Lucina Q Uddin. "Complex relationships between structural and functional brain connectivity." *Trends in cognitive sciences*, **17**(12):600–602, 2013.

[VCR11] Serge Vulliemoz, David W Carmichael, Karin Rosenkranz, Beate Diehl, Roman Rodionov, Matthew C Walker, Andrew W McEvoy, and Louis Lemieux. "Simultaneous intracranial EEG and fMRI of interictal epileptic discharges in humans." *Neuroimage*, **54**(1):182–190, 2011.

[VP10] Martijn P Van Den Heuvel and Hilleke E Hulshoff Pol. "Exploring the brain network: a review on resting-state fMRI functional connectivity." *European neuropsychopharmacology*, **20**(8):519–534, 2010.

[WKC19] Robert C Wykes, Hui Ming Khoo, Lorenzo Caciagli, Hal Blumenfeld, Peyman Golshani, Jaideep Kapur, John M Stern, Andrea Bernasconi, Stefanie Dedeurwaerdere, and Neda Bernasconi. "WONOEP appraisal: Network concept from an imaging perspective." *Epilepsia*, **60**(7):1293–1305, 2019.

[WWH11] Christopher Wilke, Gregory Worrell, and Bin He. "Graph analysis of epileptogenic networks in human partial epilepsy." *Epilepsia*, **52**(1):84–93, 2011.

[XJY18] Xinying Xing, Junzhong Ji, and Yao Yao. "Convolutional neural network with element-wise filters to extract hierarchical topological features for brain networks." In *2018 IEEE International Conference on Bioinformatics and Biomedicine (BIBM)*, pp. 780–783. IEEE, 2018.

[YTG04] Seung-Schik Yoo, Ion-Florin Talos, Alexandra J Golby, Peter McL Black, and Lawrence P Panych. "Evaluating requirements for spatial resolution of fMRI for neurosurgical planning." *Human brain mapping*, **21**(1):34–43, 2004.

[ZK17] Matthew M Zack and Rosemarie Kobau. "National and state estimates of the numbers of adults and children with active epilepsy—United States, 2015." *MMWR. Morbidity and mortality weekly report*, **66**(31):821, 2017.

[ZP14] Zisheng Zhang and Keshab K Parhi. "Seizure detection using wavelet decomposition of the prediction error signal from a single channel of intra-cranial EEG." In *2014 36th annual international conference of the IEEE engineering in medicine and biology society*, pp. 4443–4446. IEEE, 2014.

[ZPI17] Jun-Yan Zhu, Taesung Park, Phillip Isola, and Alexei A Efros. "Unpaired image-to-image translation using cycle-consistent adversarial networks." In *Proceedings of the IEEE international conference on computer vision*, pp. 2223–2232, 2017.

[ZWW19] Tong Zhao, Haixiang Wang, Kang Wang, Xiaojiao Yang, Wenjing Zhou, and Bo Hong. "Cross-modal Consistency of Epileptogenic Network in SEEG and Resting-state fMRI." In *2019 9th International IEEE/EMBS Conference on Neural Engineering (NER)*, pp. 953–956. IEEE, 2019.